Received: 15 December 2022 | Revised: 7 February 2023 | Accepted: 18 February 2023

DOI: 10.1111/tra.12883

RESEARCH ARTICLE

Traffic WILEY

N-BAR and F-BAR proteins—endophilin-A3 and PSTPIP1—control clathrin-independent endocytosis of L1CAM

Camille Lemaigre[1] | Apolline Ceuppens[1] | Cesar Augusto Valades-Cruz[2,3,4] | Benjamin Ledoux[1] | Bastien Vanbeneden[1] | Mujtaba Hassan[5] | Fredrik R. Zetterberg[6] | Ulf J. Nilsson[5] | Ludger Johannes[2] | Christian Wunder[2] | Henri-François Renard[7] | Pierre Morsomme[1]

[1]UCLouvain, Louvain Institute of Biomolecular Science and Technology, Group of Molecular Physiology, Louvain-la-Neuve, Belgium

[2]Institut Curie, Université PSL, U1143 INSERM, UMR3666 CNRS, Cellular and Chemical Biology unit, Paris, France

[3]SERPICO Project Team, UMR144 CNRS Institut Curie, PSL Research University, Paris, France

[4]SERPICO Project Team, Inria Centre Rennes-Bretagne Atlantique, Campus Universitaire de Beaulieu, Rennes, France

[5]Department of Chemistry, Lund University, Lund, Sweden

[6]Galecto Biotech AB, Sahlgrenska Science Park, Gothenburg, Sweden

[7]UNamur, NARILIS, Unité de recherche en biologie cellulaire animale (URBC), Namur, Belgium

Correspondence
Pierre Morsomme, UCLouvain, Louvain Institute of Biomolecular Science and Technology, Group of Molecular Physiology, Croix du Sud 4-5, B-1348, Louvain-la-Neuve, Belgium.
Email: pierre.morsomme@uclouvain.be

Henri-François Renard, UNamur, NARILIS, Unité de recherche en biologie cellulaire animale (URBC), Rue de Bruxelles 61, B-5000 Namur, Belgium.
Email: henri-francois.renard@unamur.be

Funding information
Agence Nationale de la Recherche; Fédération Wallonie-Bruxelles; Fonds pour la Formation à la Recherche dans l'Industrie et dans l'Agriculture; Fonds National de la Recherche Scientifique, Grant/Award Number: CDR-J.0119.19; Communauté française de Belgique–Actions de Recherches Concertées, Grant/Award Number: 17/22-085; Fonds de

Abstract

Recent advances in the field demonstrate the high diversity and complexity of endocytic pathways. In the current study, we focus on the endocytosis of L1CAM. This glycoprotein plays a major role in the development of the nervous system, and is involved in cancer development and is associated with metastases and poor prognosis. Two L1CAM isoforms are subject to endocytosis: isoform 1, described as a clathrin-mediated cargo; isoform 2, whose endocytosis has never been studied. Deciphering the molecular machinery of isoform 2 internalisation should contribute to a better understanding of its pathophysiological role. First, we demonstrated in our cellular context that both isoforms of L1CAM are mainly a clathrin-independent cargo, which was not expected for isoform 1. Second, the mechanism of L1CAM endocytosis is specifically mediated by the N-BAR domain protein endophilin-A3. Third, we discovered PSTPIP1, an F-BAR domain protein, as a novel actor in this endocytic process. Finally, we identified galectins as endocytic partners and negative regulators of L1CAM

Abbreviations: ALCAM, activated leukocyte cell adhesion molecule; BAR, Bin/Amphiphysin/Rvs; PSTPIP, proline-serine-threonine phosphatase-interacting protein; CHC, clathrin heavy chain; CIE, clathrin-independent endocytosis; CLIC, clathrin-independent carrier; CME, clathrin-mediated endocytosis; CTxB, cholera toxin, B subunit; EFC, extended FC; Endo, endophilin; FCH, Fer/CIP4 homology; FEME, fast endophilin-mediated endocytosis; Gal, galectin; GEEC, GPI-anchored protein early endosomal compartment; GL-Lect, glycolipids-lectins; GSL, GlycoSphingoLipid; KIF, kifunensine; L1CAM, L1 cell adhesion molecule; LacNAc, N-acetyl-D-lactosamine; LLSM, lattice-light sheet microscopy; PAPA, pyogenic sterile arthritis, pyoderma gangrenosum and acne; PEST, proline (P), glutamic acid (E), serine (S) and threonine (T); PI(4,5)P2, phosphatidylinositol 4,5-bisphosphate; STxB, Shiga toxin, B subunit; Tf, transferrin; TIRF, total internal reflection fluorescence; WASP, Wiskott Aldrich syndrome protein.

Henri-François Renard and Pierre Morsomme have jointly supervised this work.

La Recherche Scientifique - FNRS, Grant/Award Number: MIS-F.4540.21; French National Research Agency, Grant/Award Number: ANR-10 INBS-04-07; Labex DCBiol, Grant/Award Number: ANR-11-LABX-0043; Labex Cell(n)Scale, Grant/Award Number: ANR-11-LABX-0038; Idex PSL, Grant/Award Number: ANR-10-IDEX-0001-02

endocytosis. In summary, the interplay of the BAR proteins endophilin-A3 and PSTPIP1, and galectins fine tune the clathrin-independent endocytosis of L1CAM.

KEYWORDS

BAR domain proteins, Clathrin-independent endocytosis, endophilin-A3, galectin, L1CAM, PSTPIP1

1 | INTRODUCTION

Endocytosis is a key cellular process for maintaining plasma membrane homeostasis. A quick look in the literature is enough to grasp the high diversity and complexity of endocytic pathways.[1] Among them, CME (Clathrin-Mediated Endocytosis) is the best characterised mechanism, where clathrin molecules are recruited to the plasma membrane, form a coat to deform the cargo-enriched endocytic site and help to generate endocytic vesicles.[2] Less well characterised are CIE (Clathrin-Independent Endocytosis) mechanisms, in which membrane curvature is driven by other molecular players, such as BAR domain proteins. BAR domain proteins sense or induce membrane curvature, thanks to the ability of their curved-shape oligomers to interact with membranes.[3–6] Several BAR domain proteins have already been described to function in different endocytic mechanisms. For example, in CME, FCHo1 and FCHo2 initiate membrane bending.[7–9] In CIE, endophilin-A2 plays a major role in FEME (Fast Endophilin-Mediated Endocytosis) and in the uptake of bacterial toxins,[10,11] GRAF 1 is involved in the CLIC/GEEC (Clathrin-Independent Carrier/GPI-anchored protein Early Endosomal Compartment) pathway[7,12,13] as well as PICK1 and IRSp53.[14] More recently, we described a CIE mechanism mediated by endophilin-A3 (endoA3) which controls CD166/ALCAM (Activated Leukocyte Cell Adhesion Molecule) internalisation.[15,16]

The endophilin A (endoA) subfamily belongs to the N-BAR proteins, which contain an N-terminal BAR domain, a middle variable region, and a C-terminal SH3 domain. In addition, they possess an N-terminal amphipathic helix (main characteristic of the N-BAR family), which can insert into the membrane to amplify curvature[3,4,17–20] or help proteins to be recruited at the membrane.[11] EndoA subfamily is composed of three isoforms: endoA1, -A2 and -A3. These proteins are known to act in both clathrin-dependent and -independent endocytosis. Initially, endoAs were considered as redundant given their high sequence similarity. For example, in CME, endoAs were shown to be recruited to the neck of clathrin-coated pits, acting like a support for uncoating after membrane fission.[21,22] In CIE, endoAs were discovered as key molecular players in FEME with their abilities to be a cargo recruitment adaptor and to curve membrane.[10] Later on, it was demonstrated that among the three endoAs, A2 isoform was the most important for FEME.[23] Always in CIE, endoA2 has been shown to form a scaffold around plasma membrane invaginations induced by Shiga toxin, which primes membrane tube for fission under the pulling forces of molecular motors.[11] Finally, endoA3 isoform was described as a major player in CD166/ALCAM internalisation.[16] These different studies depict the isoform-specific functions of endoAs in distinct endocytic mechanisms.

In the F-BAR subfamily, several candidates have also been involved in CME, such as FCHo1 and FCHo2,[7–9] as well as in CIE, for example, FBP17 and CIP4, playing a role in early stages upon FEME activation.[23,24] F-BAR domain proteins are characterised by the presence of the F-BAR domain, also called EFC (Extended FC) domain, composed of a FCH (Fer/CIP4 homology) domain with a nearby coiled-coil region.[25] This family usually shows a more extended shape and a shallower curvature.[19,26] However, to date, several F-BAR domain proteins have never been studied in the context of endocytosis. Among them, PSTPIP (proline-serine-threonine phosphatase interacting protein) proteins are particularly interesting candidates (see below in our study). These proteins exist in two isoforms: PSTPIP1 and -2. PSTPIP1 contains a typical F-BAR domain in the N-terminal part, a PEST sequence (enriched in proline [P], glutamic acid [E], serine [S] and threonine [T]) and a C-terminal SH3 domain.[27,28] Compared with PSTPIP1, PSTPIP2 (also called MAYP for Macrophage actin-associated tyrosine phosphorylated protein) lacks the SH3 domain[29,30] and is not able to interact with WASP (Wiskott Aldrich syndrome protein), an actin cytoskeleton regulator.[31] Both PSTPIP proteins regulate filopodia formation in macrophages and F-actin cytoskeleton, and their mutated versions lead to autoinflammatory diseases.[32–34] Mutations of PSTPIP1 are responsible for a pathology called the PAPA syndrome (Pyogenic sterile Arthritis, Pyoderma gangrenosum and Acne).[34,35] Mutated PSTPIP2 results in macrophage-mediated autoinflammatory diseases.[31] Those cytosolic proteins are able to bind to the phospholipids PI(4,5)P2 (Phosphatidylinositol 4,5-bisphosphate) and to induce tubulation in liposomes in vitro.[25] In this work, we focused on the role of PSTPIP1.

Next to cytosolic factors involved in the construction of endocytic pits, cargoes are also important actors in endocytosis. In the current work, we focused on L1CAM (L1 Cell Adhesion Molecule), a transmembrane glycoprotein belonging to the immunoglobulin-like family. It is composed of (i) a large extracellular domain, divided into six immunoglobulin-like domains and five fibronectin-III domains, (ii) a transmembrane span and (iii) a short cytosolic tail of ~110 amino acids.[36–38] The protein contains 22 potential N-glycosylation sites and is therefore heavily glycosylated. L1CAM was first identified in neurons, and described as essential during brain development and maturation.[39] L1CAM undergoes alternative splicing generating three different isoforms: (1) the full-length version (called isoform 1 hereafter); (2) the short-version lacking exon 2 and 27 (called isoform 2 hereafter) and (3) the soluble version without the exon 25 (transmembrane region, not considered in the current work). The isoform 1 is expressed in neurons and Schwann cells.[40] The isoform 2 is also found in Schwann cells, but also haematopoietic and epithelial cells.[41,42] The third isoform was discovered in epithelial cells.[43] L1CAM is also overexpressed in several cancers where it promotes invasion and motility, and correlates with poor prognosis.[44,45] Interestingly, early studies

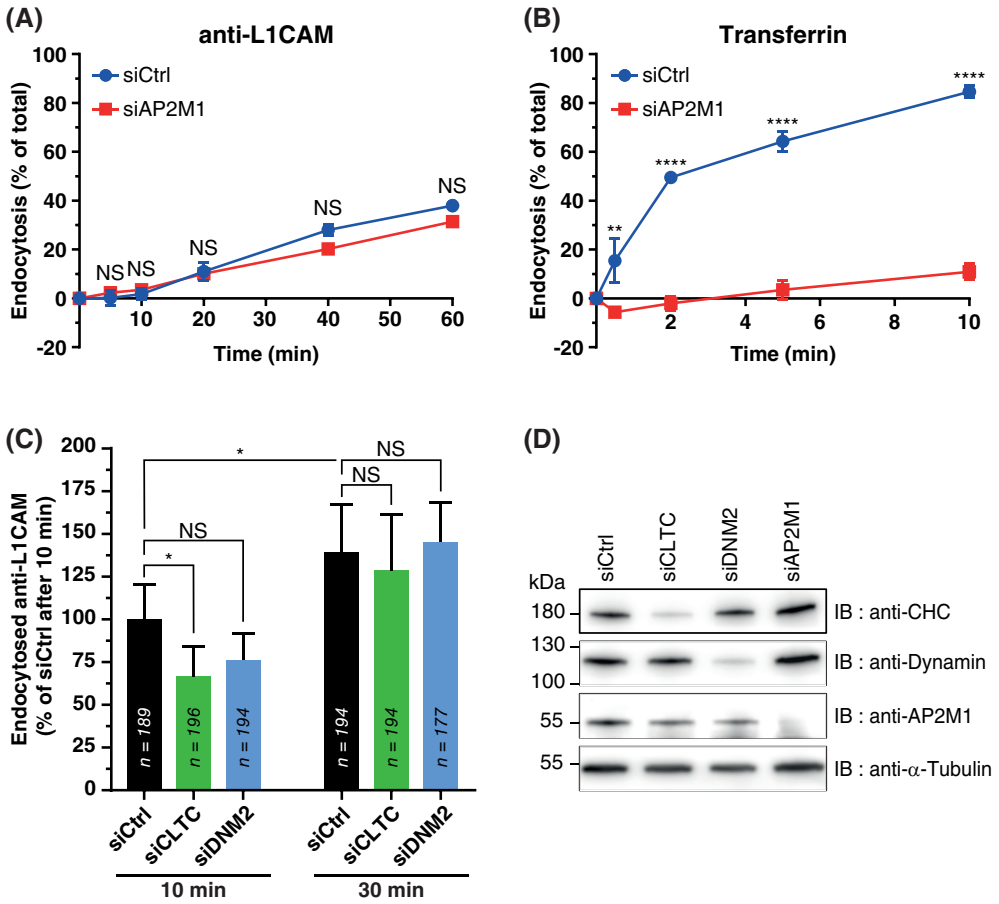

FIGURE 1 L1CAM isoform 2 is preferentially endocytosed in a clathrin-independent manner. Anti-L1CAM antibody uptake assays in HeLa cells treated for 72 h with indicated siRNAs: control (siCtrl), μ2-adaptin (siAP2M1), clathrin heavy chain (siCLTC) or dynamin-2 (siDNM2). (A, B) Uptake measurement by loss of surface assays in flow cytometry, upon μ2-adaptin depletion (AP2M1). Cargoes are L1CAM (A) or Transferrin (B). Three independent experiments. NS, not significant; $^{**}p < 0.01$; $^{****}p < 0.0001$ (two-way ANOVA with Bonferroni's multiple comparison test). (C) Continuous uptake of L1CAM for 10 and 30 min. Internal fluorescence was quantified from confocal images and plotted as the relative percentage of siCtrl (after 10 min) condition. *N* cells, three independent experiments. NS, not significant. $^{*}p < 0.05$ (Kruskal–Wallis test with Dunn's multiple comparison post hoc test, two-tailed). (D) Western-blots against clathrin heavy chain (anti-CHC), dynamin (anti-Dynamin) and μ2-adaptin (anti-AP2M1) highlight siRNA efficacy. α-tubulin was used as loading control. Data are mean ± SEM (A, B) or median ± 95% CI (C).

have proposed that the isoform 1 is endocytosed through CME, thanks to the motif YRSL present in the cytosolic tail.[46,47] This motif allows the interaction with the μ2-subunit of AP2 complex, involved in the uptake of cargoes via CME. Interestingly, isoform 2 lacks this motif, partially encoded by the exon 27 (YRSLE), but its trafficking properties have never been explored. The absence of the tyrosine motif in isoform 2 makes it a potential cargo candidate for a CIE mechanism.

In the current study, we focused on the endocytosis of the isoforms 1 and 2 of L1CAM. First, we demonstrated that the isoform 2, lacking the tyrosine motif, is preferentially endocytosed in a clathrin-independent manner, and more specifically through the endoA3-mediated mechanism. In addition, we discovered that PSTPIP1, a F-BAR domain protein, is a novel molecular player in this endocytic mechanism. Surprisingly, we observed that isoform 1 uptake is not strictly dependent on CME in our cellular model, bringing some nuance to the conclusions obtained in early studies. Interestingly, both isoforms 1 and 2 rely partially on endoA3 for their endocytosis. Finally, we identified several galectins as endocytic partners of L1CAM. Altogether, our data provide new knowledge on endoA3-mediated CIE with the identification of a new cargo, L1CAM and a new cytosolic actor, the F-BAR protein PSTPIP1. Our study also brings a more nuanced perspective on the uptake mechanism of L1CAM, which was initially considered as a CME cargo. Our results contribute to decipher the molecular mechanism of L1CAM internalisation and to better understand its physiopathological role.

2 | RESULTS

2.1 | L1CAM isoform 2 is preferentially endocytosed through CIE

For the study of the endocytosis of L1CAM isoform 2, we used HeLa and U2OS cell lines. By performing PCR on cDNA and sequencing the PCR products, we confirmed that these cell lines express solely the

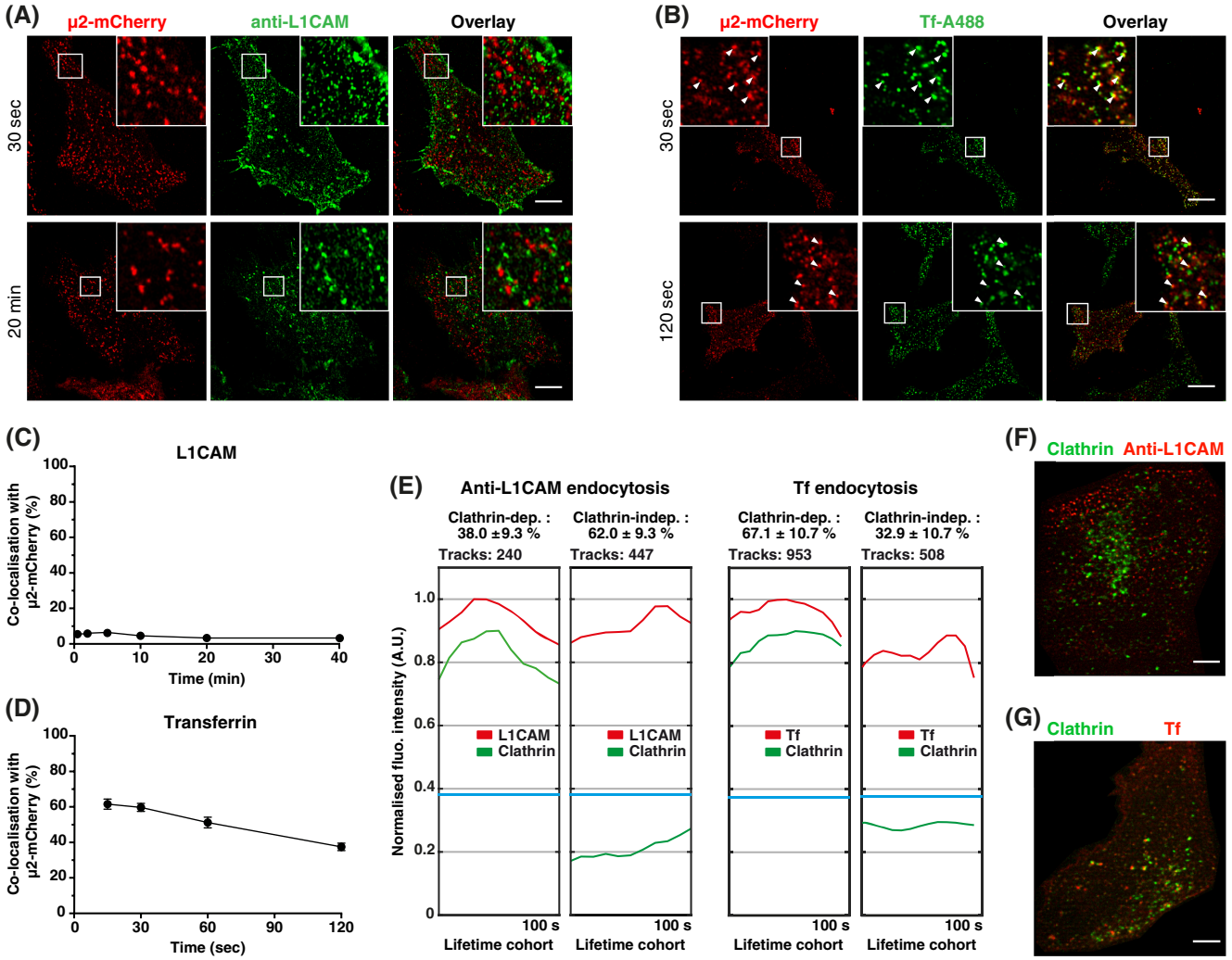

FIGURE 2 The majority of endocytic carriers of L1CAM isoform 2 are devoid of CME markers. Uptake experiments of anti-L1CAM antibody or Transferrin (Tf) in cells expressing fluorescently labelled CME markers. (A–D) Continuous uptake in HeLa cells transiently expressing mCherry-tagged μ2-adaptin (red). Cargoes (green) are L1CAM (A) and Tf (B). Representative Airyscan images from three independent experiments are shown at the indicated time points (A, B). Graphs show quantifications of co-localisation with μ2-adaptin at different time points of uptake of anti-L1CAM antibody (C) or Alexa Fluor 488-tagged Tf (Tf-A488, D). $n = 15$ cells, three independent experiments. (E–G) Endocytosis imaged by LLSM on live U2OS cells. Full 3D volume of 60 planes per cell acquired within 3 s. (E) Average endocytic normalised intensity tracks and classification of endocytic events for anti-L1CAM and Tf uptake. Endogenous genome-edited CLTA-mRFP (green); cargo (red). Lifetime cohorts of endocytic trajectories show a "dome"-shaped intensity profile of cargoes and co-tracking or not with clathrin. Blue horizontal line reflects the threshold for clathrin fluorescence intensity. Nine experiments. (F, G) 2D projections of acquired 3D stacks of cargo (red) and clathrin (green). Representative of nine experiments per cargo. Data are mean ± SEM (C, D) or mean ± SD (E). Scale bars, 10 μm (A, B), 5 μm (F, G).

second isoform of L1CAM (Figure S1). In order to explore the role of CME in the process, we first measured the uptake of L1CAM antibodies over time upon μ2-adaptin depletion, using loss-of-surface assays. As explained above, L1CAM isoform 2 lacks the tyrosine motif allowing binding to the AP2 complex. As expected, the depletion of μ2-adaptin had no effect on the uptake of this L1CAM isoform (Figure 1A). As a control, we measured the internalisation of transferrin, its receptor being considered as a canonical cargo of CME.[48–50] Transferrin uptake was strongly inhibited when μ2-adaptin was silenced (Figure 1B). Next, using continuous antibody uptake assays, we measured the uptake of L1CAM isoform 2 upon clathrin-heavy chain and dynamin-2 depletion, after 10 and 30 min. Of note, clathrin heavy chain and dynamin-2 are well-described key players in CME.[51–54] Dynamin-2 depletion did not affect significantly L1CAM isoform 2 endocytosis (Figure 1C). However, at the short time point (10 min), we could observe a significant decrease (±35%) of L1CAM isoform 2 internalisation upon clathrin heavy chain depletion, which is no longer observed at the later time point (30 min) (Figure 1C). This suggests that L1CAM can still be partially endocytosed with the help of clathrin, and this is particularly visible at early time points. Of note, western blot analysis confirmed the efficacy of siRNA used for the depletions (Figure 1D).

Next, we performed co-localisation studies on cells transiently expressing mCherry-tagged μ2-adaptin, at several time points of L1CAM antibody endocytosis, using super resolution Airyscan confocal

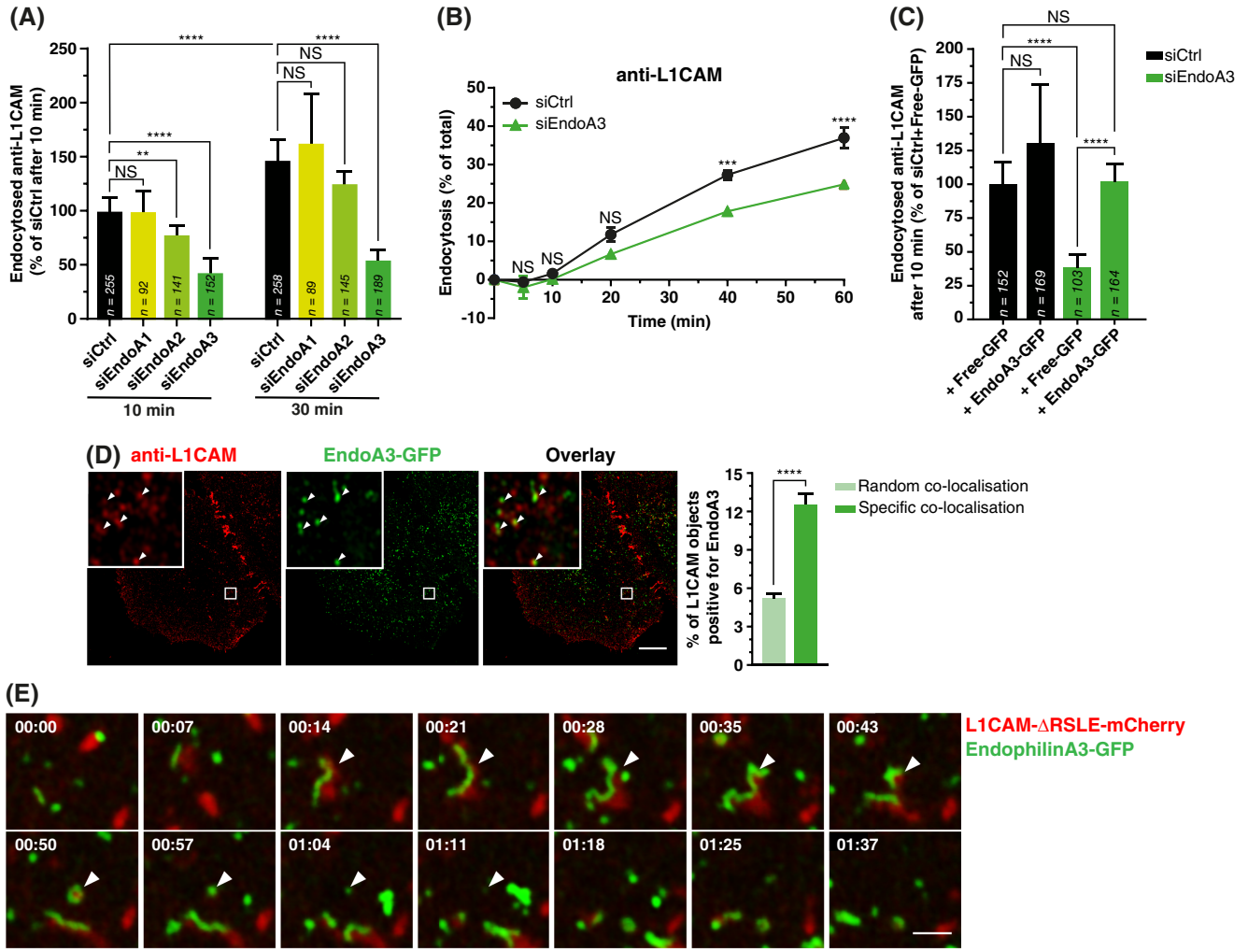

FIGURE 3 L1CAM isoform 2 is a new cargo of endoA3-mediated CIE. (A–C) L1CAM uptake in HeLa cells. Anti-L1CAM antibody uptake experiments in cells treated for 72 h with negative control siRNA (siCtrl) or siRNAs against endophilin-A1 (siEndoA1), endophilin-A2 (siEndoA2), or endophilin-A3 (siEndoA3). (A) Continuous uptake after 10 and 30 min. Internal fluorescence was quantified from confocal images and plotted as the relative percentage of siCtrl (after 10 min) condition. *n* cells. Number of independent experiments: five for siCtrl, two for siEndoA1, three for siEndoA2 and siEndoA3. NS, not significant. $^{**}p < 0.01$. $^{****}p < 0.0001$ (Kruskal–Wallis test with Dunn's multiple comparison post hoc test, two-tailed). (B) Uptake by loss-of-surface assays in flow cytometry. Four independent experiments. NS, not significant; $^{***}p < 0.001$; $^{****}p < 0.0001$ (two-way ANOVA with Bonferroni's multiple comparison test). (C) Uptake rescue experiments. siRNA-treated cells were further transfected with plasmids allowing transient expression of siRNA-resistant free GFP or EndoA3-GFP. Continuous uptake after 10 min. Internal fluorescence was quantified from confocal images and plotted as the relative percentage of siCtrl + Free-GFP condition. *n* cells. Number of independent experiments: two for siEndoA3 + Free-GFP, three for all other conditions. NS, not significant; $^{****}p < 0.0001$ (Kruskal–Wallis test with Dunn's multiple comparison post hoc test, two-tailed). (D, E) Co-localisation experiments on fixed (D) and living (E) cells stably expressing GFP-tagged endophilin-A3 (green). (D) Continuous uptake of anti-L1CAM antibody (red) for 10 min. White arrows on representative images show co-localisation events. Graph shows quantification of co-localisation. $n = 30$ cells, three independent experiments. $^{****}p < 0.0001$ (two-tailed unpaired Mann–Whitney *t* test). (E) Transient expression of mCherry-tagged L1CAM-ΔRSLE (red). Representative time series of live Airyscan confocal microscopy. White arrow highlights the dynamic association of both proteins. See Movie S5. Data are median ± 95% CI (A, C) or mean ± SEM (B, D). Scale bars, 10 μm (D), 1 μm (E).

microscopy (Figure 2A–D). Interestingly, very little co-localisation between L1CAM and μ2-adaptin (<5%) was observed all along the experiment (from 30 s to 40 min) (Figure 2A, C). As a control, we observed a high level of co-localisation between transferrin and μ2-adaptin at early time points (±60%), which decreased over time due to endocytosis of the cargo (Figure 2B, D). These data support the hypothesis that L1CAM isoform 2 is a clathrin-independent cargo.

To obtain a more quantitative and statistical view of the proportion of endocytic events of L1CAM isoform 2 associated with clathrin, we used lattice light-sheet microscopy to track the endocytic vesicles in the whole 3D volume of living cells. This approach was successfully used in a previous study.[16] Briefly, we followed the uptake of fluorescently labelled anti-L1CAM antibody in genome-edited clathrin-mRFP U2OS cells (Figure 2E–G and Movies S1–S4). This experiment showed

that 62% of L1CAM isoform 2 endocytic events are devoid of clathrin (Figure 2E), even if some co-localisation events could be observed (Figure 2F and Movies S1 and S2). By contrast, transferrin endocytosis showed 67% of clathrin-dependent events (Figure 2E) and many more co-localisations events were noticed (Figure 2G and Movies S3 and S4).

Taken together, our data clearly show that L1CAM isoform 2 is preferentially endocytosed through a clathrin-independent mechanism. A limited but significant fraction of L1CAM (38%) remains endocytosed in clathrin-positive structures.

2.2 | Endophilin-A3 controls the CIE of L1CAM isoform 2

In order to decipher the molecular features of the CIE mechanism of L1CAM isoform 2, we performed co-localisation experiments with some well-described CIE markers: bacterial toxins (Cholera, Shiga) and endophilin-A proteins. First, we did not observe L1CAM on plasma membrane tubules induced by Cholera and Shiga toxin B subunits (CTxB and STxB, respectively; Figure S2A, B). Next, we carried out anti-L1CAM antibody uptake experiments in cells depleted for EndoA1, -A2 or -A3 (Figure 3A). Interestingly, L1CAM uptake was significantly reduced upon silencing of endoA3 (more than 55% after 10 and 30 min), but not of the two other A1 and A2 isoforms (Figure 3A). The involvement of endoA3 was further confirmed via loss-of-surface assays in flow cytometry using the same antibody (Figure 3B). Finally, we performed rescue experiments in conditions similar to Figure 3A, by expressing a siRNA-resistant GFP-tagged endoA3 construct in cells where endogenous endoA3 was depleted by RNA silencing (Figure 3C). Strikingly, uptake was completely rescued by expression of the endoA3-GFP construct, as compared with the expression of free GFP alone (Figure 3C). Altogether, these datasets demonstrate a functional involvement of endoA3 in the uptake of L1CAM isoform 2, suggesting that the protein is a new cargo of the previously described endoA3-mediated CIE mechanism.[16]

Besides functional tests, we carried out co-localisation experiments to further confirm the role of endoA3 in the uptake of L1CAM isoform 2. First, super resolution images obtained after 10 min antibody uptake with Airyscan technology revealed clear co-localisation events between the two proteins (Figure 3D). We further confirmed this association by live-cell imaging using the same microscopy technology. For this purpose, we designed a mCherry-tagged L1CAM-ΔRSLE construct, mimicking the cytosolic tail of isoform 2. As previously explained, these four amino acids, encoded by exon 27 and present in the cytosolic tail of L1CAM isoform 1, allow the binding of the AP-2 complex. We observed a clear dynamic association between GFP-tagged endoA3 (stable expression) and L1CAM-ΔRSLE-mCherry (transient expression) in cells co-expressing the two proteins (Figure 3E and Movie S5). Interestingly, we were able to observe the formation of vesicular structures containing L1CAM and wrapped with endoA3, followed by the disappearance of both signals (Figure 3E and Movie S5). To confirm that those structures are endocytic events, we performed live-cell TIRF microscopy (Movie S6). Of note, we visually selected cells that we considered as low or medium expressing cells in order to minimise over-expression artefacts. Upon high expression, we have observed the formation of bigger and more stable L1CAM-positive structures (more than 1 μm diameter, compared with previously observed structures <0.5 μm) surrounded by endoA3-GFP (Figure S3 and Movie S7). Altogether, these results confirm the specific and dynamic association between endoA3 and L1CAM isoform 2 during endocytosis.

2.3 | The F-BAR domain protein PSTPIP1 is a novel molecular player in endoA3-mediated CIE involved in the uptake of L1CAM isoform 2

To go deeper into the molecular mechanism of endocytosis, we performed a wide functional screening with siRNAs against most BAR domain proteins, using the uptake of L1CAM as a readout (data not shown). Two major hits stood out: endoA3 as expected, and the F-BAR domain protein PSTPIP1. Interestingly, loss-of-surface experiments in flow cytometry confirmed the involvement of PSTPIP1 in L1CAM isoform 2 uptake over time (Figure 4A). The role of PSTPIP1 was also observed in direct uptake experiments of anti-L1CAM antibodies, where antibody accumulation into cells was reduced by 34% upon PSTPIP1 depletion (Figure 4B). Of note, we confirmed the efficiency of the siRNA smartpool against PSTPIP1 by qRT-PCR (Figure S4A). We also confirmed that the decrease of uptake of L1CAM isoform 2 was not due to off-targets of siRNAs by monitoring the effect of two separate sequences (Figure S4B, as compared with Figure 4B). Next, we combined the silencing of endoA3 and PSTPIP1 to look for a potential additive effect on L1CAM endocytosis (Figure 4C). Interestingly, the combination did not lead to a stronger reduction of L1CAM uptake as compared with the depletion of endoA3 alone. This suggests that endoA3 and PSTPIP1 both contribute to the same endocytic route.

Next, we further studied the involvement of PSTPIP1 in the endocytic mechanism via co-localisation experiments with L1CAM isoform 2 or endoA3, using super resolution Airyscan confocal and TIRF microscopy. First, we performed anti-L1CAM antibody uptake experiments in cells expressing GFP-tagged PSTPIP1. In line with the previous results obtained with endoA3 (Figure 3D), we observed a similar degree of co-localisation between L1CAM isoform 2 and PSTPIP1 (Figure 4D). Next, using live-cell TIRF microscopy, we observed a very strong co-localisation (39%) between transiently expressed GFP-tagged PSTPIP1 and mCherry-tagged endoA3 (Figure 4E and Movie S8). From TIRF time series, we quantified the lifetime of each protein spot at the cell surface, either when they co-localise or when they do not co-localise (Figure 4F). We observed a very significant increase of the lifetime of each protein upon co-localisation—2.2-fold increase for PSTPIP1 and 1.5-fold increase for endoA3—while non-co-localising spots were much shorter lived. Interestingly, we could also determine the sequence of appearance and disappearance of protein spots at the cell surface. Remarkably, PSTPIP1 appeared 3.32 s before endoA3 and disappeared 3.14 s after

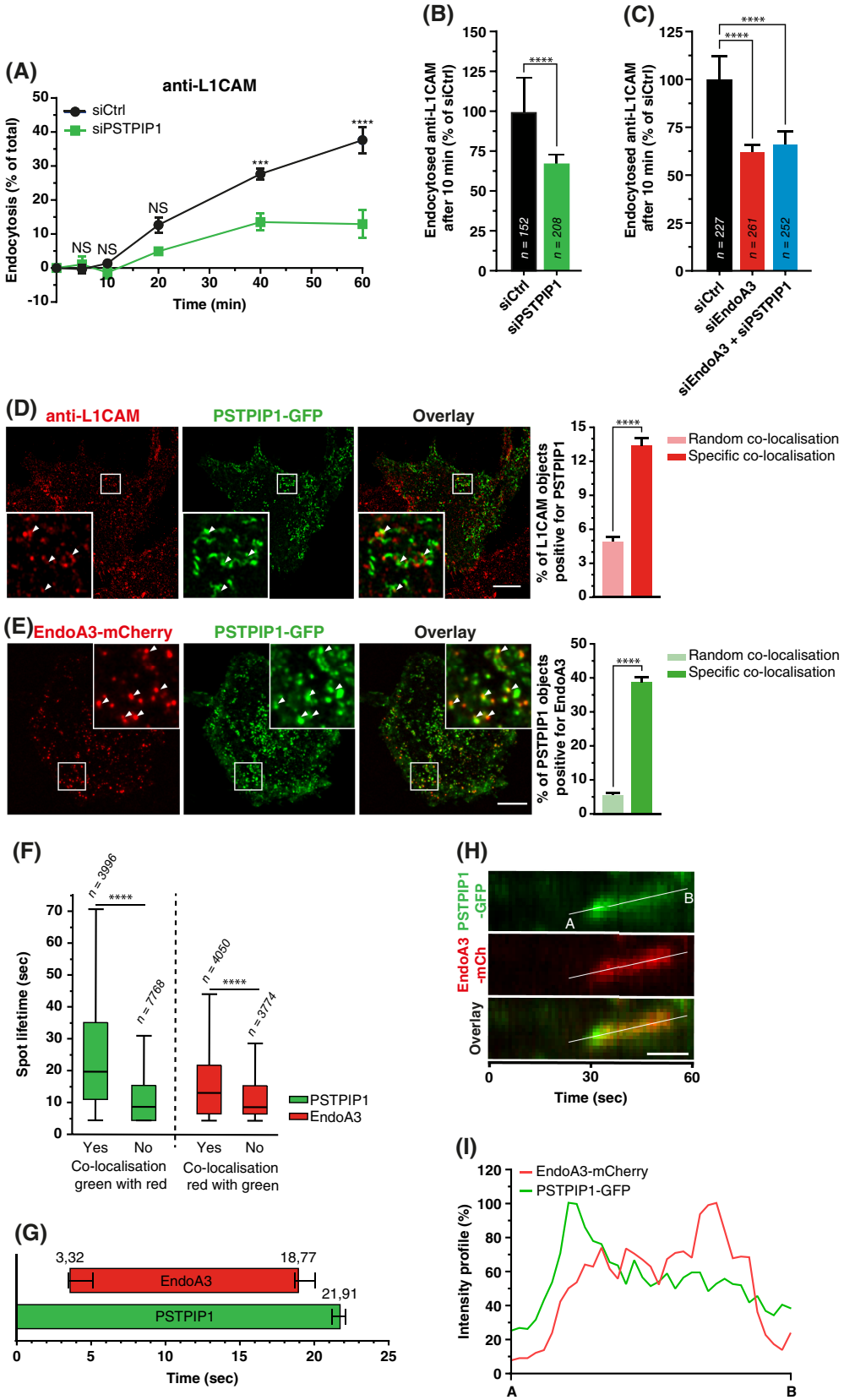

FIGURE 4 Legend on next page.

endoA3 (Figures 4G–I, S5 and Movie S9). This suggests an early role of PSTPIP1 in the endocytic process.

Based on these functional and co-localisation data, we then wondered if the two BAR domain proteins—endoA3 and PSTPIP1—and L1CAM physically interact. To answer this question, we performed pull-downs assays using the cytosolic tails of either L1CAM isoform 1 or 2 as baits, expressed from bacteria. The baits were then incubated with lysates of HeLa cells expressing either endoA3-GFP (stable) or PSTPIP1-GFP (transient). Interestingly, both L1CAM isoforms led to the efficient pull-down endoA3 and PSTPIP1 (Figure 5A, B). Of note, ezrin is known to interact with L1CAM[55] and was used as a positive control. In addition, we used endogenous endoA2 as a negative control as previously published,[16] proving again that the different endoA isoforms are not redundant and have specific functions.

Altogether, all these functional, co-localisation and physical interaction studies converge towards PSTPIP1 as a new actor in endoA3-mediated CIE involved in the uptake of L1CAM isoform 2. Interestingly, our data suggest that PSTPIP1 plays an early role in endoA3-mediated CIE.

2.4 | L1CAM isoform 1 is also a cargo of endoA3-mediated CIE

Long time ago, L1CAM isoform 1 was described as a CME cargo and is considered as such since these very early studies.[47] However, the results from our pull-down experiments show that both endoA3 and PSTPIP1, considered here as CIE markers, can also physically interact with the cytosolic tail of the isoform 1 of L1CAM. Our observations suggest thus that L1CAM isoform 1 might also be a CIE candidate. In order to test this hypothesis, we generated a HeLa cell line stably expressing GFP-tagged L1CAM isoform 1 (Figure 5C, D). As a reminder, HeLa cells do not express this isoform of L1CAM (Figure S1). From Western blot analysis using an antibody recognising both isoforms, it appears that the expression level of exogenous L1CAM isoform 1 protein in our cell line is close to the endogenous expression level of L1CAM isoform 2 (Figure 5C). In addition, GFP-tagged L1CAM isoform 1 shows a plasma membrane localisation, with an expected enrichment at the intercellular junctions (Figure 5D).

First, we performed uptake experiments with anti-L1CAM antibodies in our L1CAM isoform 1 expressing cell line, where endogenous L1CAM isoform 2 was depleted by RNA interference. We looked at the co-localisation between the antibody and clathrin heavy chain detected by immunofluorescence at early uptake time points (5 min, Figure 5E). Interestingly, we could observe weak but specific co-localisation events between the two proteins.

Next, we performed quantitative uptake assays upon depletion of clathrin heavy chain, endoA3 and combinations (Figure 5F). As in the previous experiment (Figure 5E), endogenous L1CAM isoform 2 was specifically silenced using siRNAs. Interestingly, clathrin heavy chain depletion partially inhibited L1CAM isoform 1 internalisation (45% decrease). Upon endoA3 silencing, L1CAM isoform1 endocytosis was reduced by about 27%. The combined depletion of clathrin heavy chain and endoA3 showed a reduction in uptake of the same magnitude as the depletion of clathrin heavy chain alone (46%). Of note, we verified the efficiency of the depletions by Western blot analysis (Figure 5G). In addition, we quantified the uptake of L1CAM isoform 1 uptake upon PSTPIP1 depletion and observed a signification reduction (33%) in this condition (Figure 5H), which is very similar with what we observed for L1CAM isoform 2 (Figure 4B).

Altogether, these data suggest that L1CAM isoform 1 is not strictly dependent on CME for its endocytosis and that a significant fraction of this isoform is endocytosed via endoA3-mediated CIE.

2.5 | L1CAM and galectins are endocytic partners

In this section, all experiments were performed on L1CAM isoform 2, naturally expressed in HeLa cells. We therefore use the term L1CAM instead of L1CAM isoform 2.

FIGURE 4 F-BAR protein PSTPIP1 is functionally involved in L1CAM isoform 2 endocytosis and co-localises dynamically with endoA3 at the cell surface. Experiments on HeLa cells. (A–C) Anti-L1CAM antibody uptake experiments in cells treated for 72 h with negative control siRNA (siCtrl) or siRNAs against endoA3 (siEndoA3), PSTPIP1 (siPSTPIP1) or combinations. (A) Uptake by loss-of-surface assays in flow cytometry. Three independent experiments. NS, not significant. ***$p < 0.001$. ****$p < 0.0001$ (two-way ANOVA with Bonferroni's multiple comparison test). (B, C) Continuous uptake experiments after 10 min. Internal fluorescence was quantified from confocal images and plotted as the relative percentage of siCtrl condition. *n* cells, three (B) or four (C) independent experiments. (B) Depletion of PSTPIP1 alone. ****$p < 0.0001$ (two-tailed unpaired Mann–Whitney *t* test). (C) Combined depletion of endoA3 and PSTPIP1. ****$p < 0.0001$ (Kruskal–Wallis test with Dunn's multiple comparison post hoc test, two-tailed). (D–I) Co-localisation experiments on fixed (D) and live (E–I) cells transiently expressing GFP-tagged PSTPIP1 (green). (D) Continuous uptake of anti-L1CAM antibody (red) for 10 min. White arrows on representative images show co-localisation events. Graph shows quantification of co-localisation. $n = 30$ cells, three independent experiments. ****$p < 0.0001$ (two-tailed unpaired Mann–Whitney *t* test). (E–I) Transient co-expression of mCherry-tagged endoA3 (red). (E) Representative TIRF images of living cells. Graph shows quantification of co-localisation. White arrows show co-localisation events. $n = 30$ cells, three independent experiments. ****$p < 0.0001$ (two-tailed unpaired Mann–Whitney *t* test). (F–I) Quantitative analysis of TIRF live-cell time series. (F) Spot lifetime of PSTPIP1-GFP and EndoA3-mCherry upon co-localisation or not. $n = 6$ cells, one experiment. ****$p < 0.0001$ (two-tailed unpaired Mann–Whitney test). (G) Sequence of appearance and disappearance of PSTPIP1-GFP and EndoA3-mCherry signals in co-localising tracks. All tracks were synchronised on the appearance of PSTPIP1 signal (time = 0 s). $n = 4481$ tracks from six cells, one experiment. (H) Representative kymograph of co-localising tracks quantified in 'G'. (I) Fluorescence intensity profile of both proteins, along the white line drawn on the kymograph in 'H'. Maximum fluorescence in both channels was set at 100%. Data are mean ± SEM (A, D, E) or median ± 95% CI (B, C, G). Box plots (F) show median, 25th and 75th percentiles (boxes), and data range from min to max (whiskers). Scale bars, 10 μm (D, E), 1 μm (H).

Like CD166/ALCAM,[16] L1CAM is an immunoglobulin-like protein endocytosed with the help of endoA3. As the endocytosis of CD166 is driven by Galectin-8 (Gal8),[16] we wondered if the CIE of L1CAM is also dependent on galectins and if it follows the GL-Lect (GlycoLipid-Lectin) hypothesis.[56] According to this hypothesis, glycosylated cargo proteins and glycosphingolipids (GSLs) are clustered by extracellular lectins—such as endogenous mammalian galectins—to drive plasma membrane invagination leading to endocytic pit construction. Galectins and GSLs, as well as cargo glycosylations, are thus crucial parameters in this mechanism.

First, we performed co-uptake experiments of anti-L1CAM antibody with fluorescently labelled galectins, Gal-1, -3 and -8 (Figure 6A–C). Interestingly, we observed L1CAM-containing endocytic structures positive for all three galectins, with a significantly

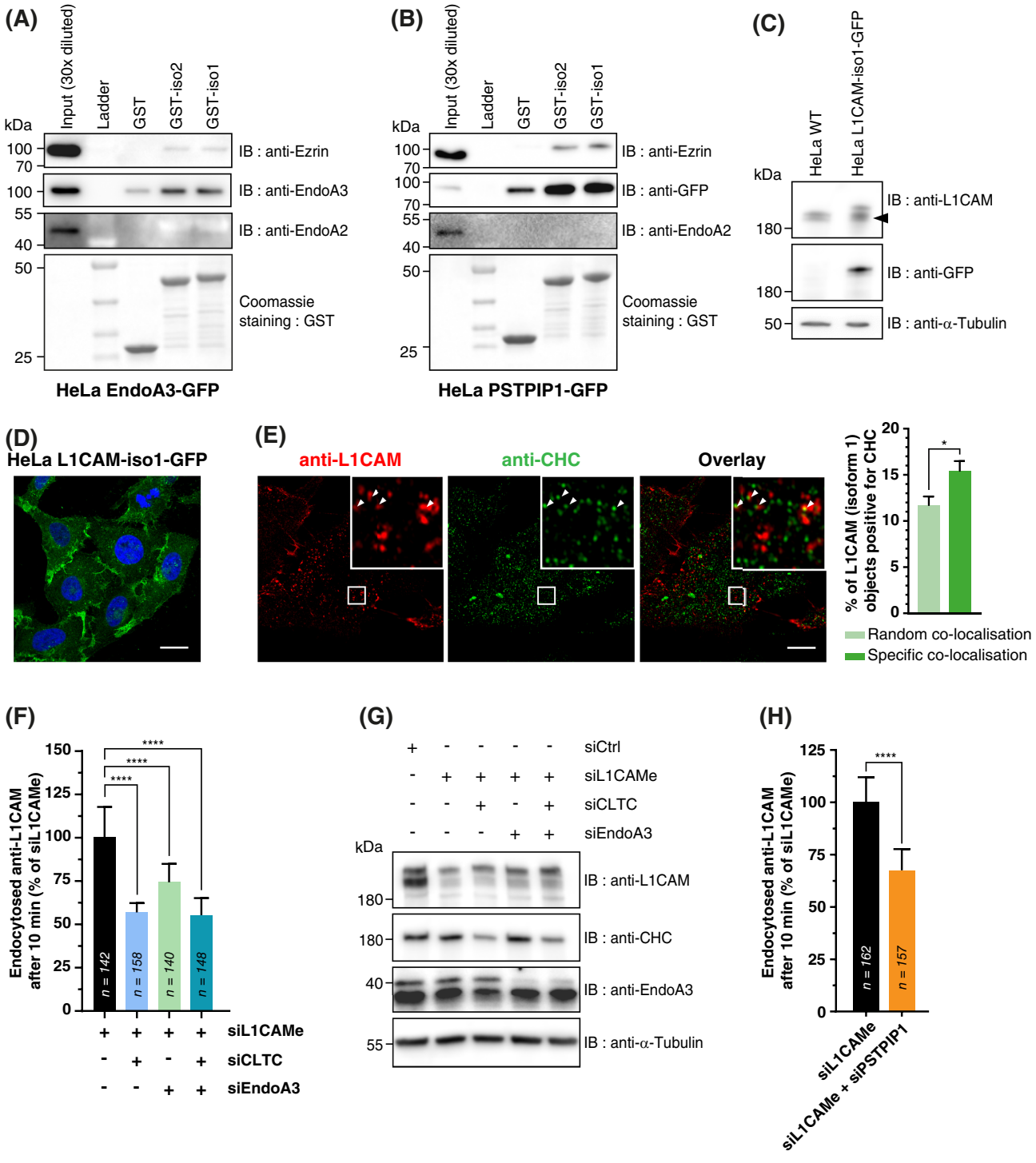

FIGURE 5 Legend on next page.

higher co-localisation for Gal-1 and Gal-8 (Figure 6D). Next, to explore the role of galectins in the endocytic process of L1CAM, we first measured the uptake efficiency in the absence of serum (which contains galectins) or in the presence of serum supplemented 10 mM LacNAc (which is a galectin competitor). Strikingly, these treatments significantly increased the uptake of L1CAM as compared with the 10% serum condition only (Figure 6E, F), in stark contrast to previously published results for CD166.[16] This result seems to indicate that a global inhibition of interaction with galectins apparently stimulates L1CAM endocytosis.

In order to dissect the role of galectins more precisely, we performed further L1CAM uptake experiments in the presence of specific galectin inhibitors. inhibitors. For this, we had at our disposal four different inhibitors: GB1490 (Gal1), GB1107 (Gal3) (compound **2h** in Reference 57, **2** in Reference 58 and **11b** in Reference 59), **19a** (Gal3 + Gal8N)[60] and **10b** (N-terminal carbohydrate recognition domain of Gal8, or Gal8N).[61] K_d values of these inhibitors are available in Table S1. First, we validated these inhibitors by measuring their dose-dependent effect on the cell surface binding of galectins at 4°C (Figure S6A, C, E, G) or on the uptake of galectins at 37°C (Figure S6B, D, F, H) by flow cytometry. These results allowed to determine efficient doses for each inhibitor, which were used in subsequent experiments where we explored how the inhibition of specific galectins affects L1CAM uptake. Strikingly, L1CAM uptake remained unaffected in the presence of any of these inhibitors or their combination (Figure 6G). This data suggests that other unidentified galectins, or combinations thereof, may be involved in the modulation of L1CAM uptake.

Endocytic mechanisms following the GL-Lect hypothesis require GSLs. Therefore, we investigated the role of these lipids in L1CAM uptake. For this purpose, we measured L1CAM endocytosis upon inhibition of GSL synthesis by Genz 123346 compound.[62,63] First, we monitored the efficiency of Genz treatment conditions by measuring the cell surface binding of fluorescently labelled STxB, which is well-known to use the globoside Gb3 (globotriaosylceramide) as a receptor.[64,65] As expected, STxB binding to Genz-treated cells was strongly decreased as compared with control cells (−87%), demonstrating the efficiency of GSL depletion (Figure S7A). However, the uptake of L1CAM remained unaffected in the same GSL depletion conditions (Figure 6H).

Finally, we explored the role of L1CAM glycosylations on the uptake process of the protein. To do this, we treated cells either with a deglycosylation enzyme—neuraminidase (removing sialic acids from complex sugars)—or with a glycosylation inhibitor—Kifunensine (mannosidase I inhibitor, generating high-mannosylated proteins). 2,3-sialylations are known to be important for N-terminal Carbohydrate Recognition Domain (CRD) of Gal8 (Gal8N) binding to glycosylated proteins, but not for Gal3 binding.[66,67] Interestingly, neuraminidase treatment led to an expected reduction of Gal8 uptake (−30%), but did not affect Gal3 uptake (Figure S7B). In the same neuraminidase treatment conditions, L1CAM uptake remained unaffected (Figure S7C). From these experiments, we can conclude that sialic acids are not crucial for the endocytosis of L1CAM. Next, we decided to induce stronger glycosylation modifications of L1CAM, using Kifunensine. Strikingly, Kifunensine treatment led to a > 50% increase of L1CAM uptake (Figure S7D). Combination of Kifunensine treatment and serum depletion led to additive effects, boosting further L1CAM endocytosis (Figure S7E). Of note, Western blot analysis confirmed that Kifunensine indeed induces the appearance of highly mannosylated forms of L1CAM, which are very sensitive to endoglycosidase H treatment (Figure S7F).

Altogether, these data suggest that although the CIE of L1CAM is mediated by endoA3, its apparent endocytic features are very different from previously studied CD166.[16] According to our current data, L1CAM uptake seems to be inhibited by galectins, while it is increased upon either general inhibition of galectin binding, or global perturbation of cargo glycosylation. In addition, perturbation of GSL synthesis had no apparent effect on L1CAM uptake. Nevertheless, L1CAM and galectins are endocytic partners, as they were found together in endocytic compartments.

FIGURE 5 L1CAM (isoform 1), clathrin-dependent cargo, is also controlled by endophilin-A3 and PSTPIP1. (A, B) GST pull-down experiments with the cytosolic tail of L1CAM isoform 1 (GST-iso1), of L1CAM isoform 2 (GST-iso2), or GST alone on lysates from HeLa cells either expressing stably GFP-tagged endoA3 (A) or transiently PSTPIP1-GFP (B). Positive control, ezrin; negative control, endophilin-A2; loading control, Coomassie staining. Representative of three independent experiments. (C, D) Generation of a stable HeLa cell line expressing GFP-tagged L1CAM isoform 1 (L1CAM-iso1-GFP). (C) Western-blots against L1CAM and GFP highlight an expression of L1CAM-iso1-GFP construct close to the endogenous protein level (black arrow). α-tubulin was used as loading control. (D) Representative Airyscan image of the stable cell line. L1CAM-iso1-GFP, green; nuclei, blue. (E) Co-localisation of L1CAM isoform 1 (red) with clathrin heavy chain (CHC) (green). HeLa cells stably expressing L1CAM-iso1-GFP were treated for 72 h with siRNAs against endogenous L1CAM. Representative Airyscan images of continuous uptake of anti-L1CAM antibody (red) after 5 min. Graph shows quantification of co-localisation. White arrows show co-localisation events. $n = 15$ cells, three independent experiments. $^{*}p < 0.05$ (two-tailed unpaired t test). (F, H) Anti-L1CAM antibody uptake experiments after 10 min on HeLa cells stably expressing L1CAM isoform 1. Endogenous L1CAM (L1CAMe, corresponding to isoform 2) was depleted using siRNAs (siL1CAMe). Cells were further treated with siRNAs against: (F) clathrin heavy chain (siCLTC), endoA3 (siEndoA3) or (H) PSTPIP1 (siPSTPIP1). Internal fluorescence was quantified from confocal images and plotted as the relative percentage of siL1CAMe condition. n cells, three independent experiments. $^{****}p < 0.0001$ (Kruskal–Wallis test with Dunn's multiple comparison post hoc test, two-tailed for 'F'; two-tailed unpaired Mann–Whitney t test for 'H'). (G) Western blots against L1CAM (anti-L1CAM), clathrin heavy chain (anti-CHC) and endoA3 (anti-EndoA3) highlight siRNA efficacy. α-tubulin was used as loading control. Data are mean ± SEM (E) or median ± 95% CI (F, H). Scale bars, 20 μm (D), 10 μm (E).

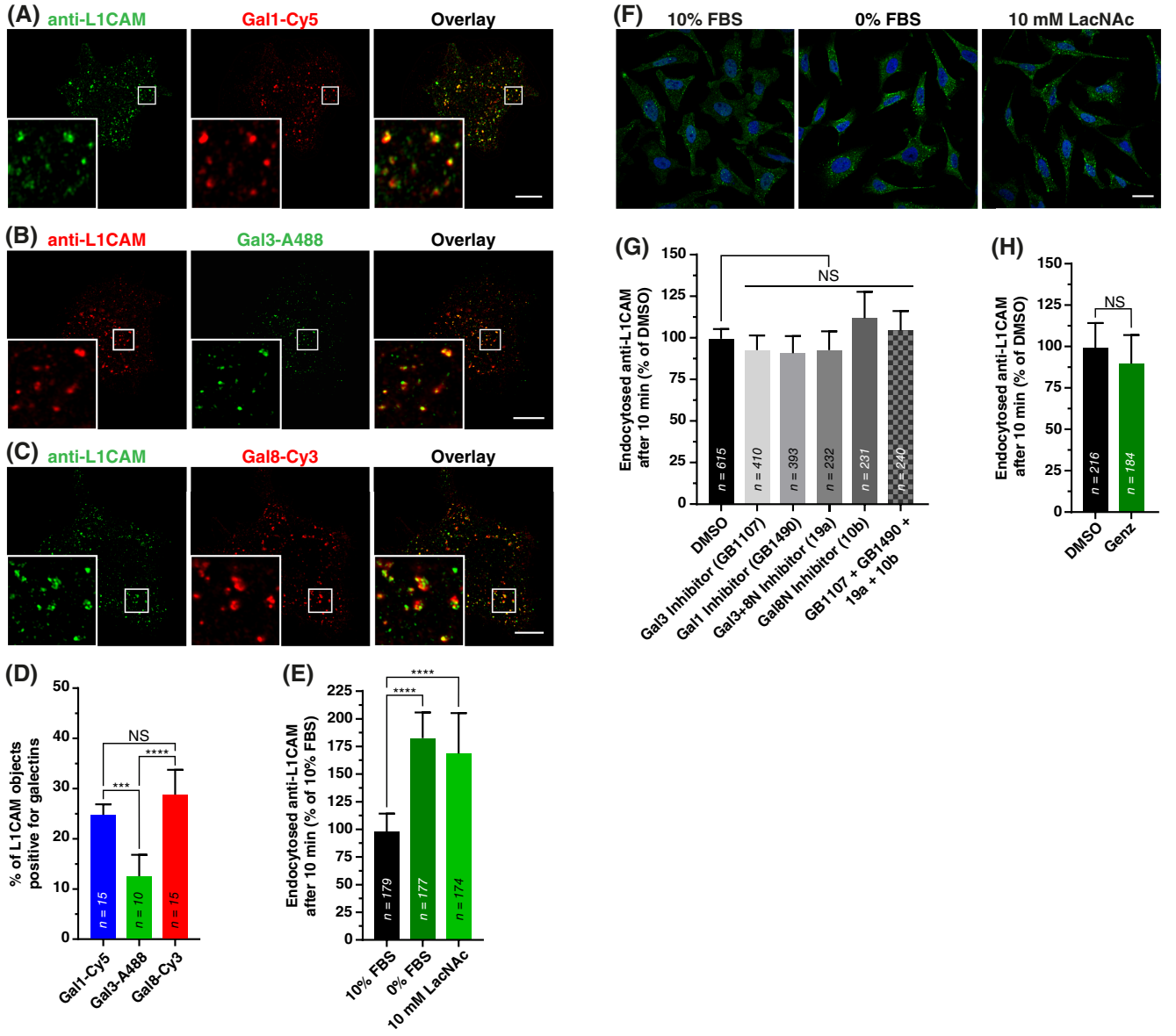

FIGURE 6 Galectins are endocytic partners of L1CAM, although GlycoLipid-Lectin hypothesis is apparently not involved in the uptake process. (A–D) Co-uptake experiments of L1CAM and galectins. Anti-L1CAM antibodies were continuously incubated for 10 min on HeLa cells in the presence of fluorescently labelled (A) Gal1 (Gal1-Cy5), (B) Gal3 (Gal3-A488), or (C) Gal8 (Gal8-Cy3). Graph shows quantification of co-localisation of L1CAM with the three galectins (D). *n* cells. Number of independent experiments: three for Gal1 and Gal8, two for Gal3. NS, not significant. ***$p < 0.001$. ****$p < 0.0001$ (ordinary one-way ANOVA with Bonferroni's multiple comparison test). (E–H) Anti-L1CAM antibody uptake in HeLa cells for 10 min. (E, F) Uptake in the absence of serum (0% FBS) or after 10 mM LacNAc treatment. (E) Internal fluorescence was quantified from confocal images and plotted as the relative percentage of 10% FBS (control) condition. *n* cells, three independent experiments. ****$p < 0.0001$ (Kruskal–Wallis test with Dunn's multiple comparison post hoc test, two-tailed). (F) Representative confocal images of the uptake assay presented in (E). Note more internal fluorescence in 0% FBS and 10 mM LacNAc conditions compare to the 10% FBS condition. (G) Uptake upon treatment with galectin inhibitors. HeLa cells were treated with DMSO (negative control) or with indicated galectin inhibitors (GB1107 and GB1490: 3 μM; 19a and 10b: 50 μM). Internal fluorescence was quantified from confocal images and plotted as the relative percentage of DMSO condition. *n* cells. Number of independent experiments: 10 for control (DMSO) condition, six for GB1107 and GB1490 conditions, and four for 19a, 10b and the combination of all inhibitors. ****$p < 0.0001$ (two-tailed unpaired Mann–Whitney *t* test). (H) Uptake under glycosphingolipid depletion. HeLa cells were treated for 48 h with the glucosylceramide synthase inhibitor Genz-122 346 (5 μM). Internal fluorescence was quantified from confocal images and plotted as the relative percentage of DMSO condition. *n* cells, three independent experiments. ****$p < 0.0001$ (two-tailed unpaired Mann–Whitney *t* test). Data are mean ± SEM. (D) or median ± 95% CI (E, G, H). Scale bars, 10 μm (A–C), 20 μm (F).

3 | DISCUSSION

In this study, we provide data demonstrating that L1CAM isoform 2 protein is mostly a CIE cargo. Interestingly, we found that both L1CAM isoforms 1 and 2 are partially dependent on endoA3 for their uptake. Surprisingly, we did not observe significant differences between isoforms 1 and 2 regarding their dependency on endoA3 or clathrin, whereas we expected isoform 1—containing a tyrosine sorting motif—to rely more stringently on CME according to previous studies.[46,47] In our hands, the endocytosis of both L1CAM isoforms was partially affected by clathrin heavy chain depletion at 10 min uptake time point (Figure 1C vs. Figure 5F). To quantify more precisely the fraction of the protein taken up in clathrin-positive and clathrin-negative endocytic carriers, lattice light-sheet microscopy and advanced quantification approaches were used. This strategy revealed that 38% of L1CAM isoform 2 endocytic events were clathrin-positive. For comparison, this is 10% more clathrin-positive endocytic events than for CD166/ALCAM cargo in our previous study.[16] While this may explain the partial effect of clathrin heavy chain depletion on L1CAM isoform 2 uptake at early time points (10 min), these data are surprising given that the YXXØ (YRSL) motif is lacking in the isoform 2. Other sorting signals recognised by cargo-selective clathrin adaptors are mentioned in the literature[68]: [DE]XXXL[LI] recognised by the α-σ2 hemicomplex of AP-2,[69,70] II (di-isoleucine) also recognised by AP-2,[71] and [FY]XNPX[YF] recognised by the PTB domain of ARH, DAB2 and NUMB.[70,72] However, none of these motifs are present in the cytosolic tail of L1CAM. How L1CAM isoform 2 can be sorted in CME carriers remains thus enigmatic and raises the question of the existence of new motifs for cargo sorting in CME, or the association of L1CAM with proteins having sorting signals. As a corollary, our observations question the functionality of the tyrosine motif in isoform 1, as no apparent difference could be detected with isoform 2 (lacking the motif).

More interestingly, our work also reveals a previously unnoticed role for the F-BAR domain protein PSTPIP1 in endoA3-mediated CIE. We observed that the depletion of both BAR domain proteins significantly reduced L1CAM isoform 1 and 2 internalisation. PSTPIP1 has never been studied in the context of endocytosis previously. However, this new function may not be so surprising. Indeed, other F-BAR domain proteins such as CIP4[25] and FBP17[73] are known to play a role in endocytosis. Thanks to their EFC domain, they bind to the membrane lipids, more precisely to PI(4,5)P2, and induce shallow curvature. Like CIP4, PSTPIP1 was shown to induce strong tubulation on liposomes.[25] All those F-BAR proteins also possess a SH3 domain capable of binding to N-WASP and dynamin-2.[25] These last two proteins form a complex present in the fission stage of CME.[74]

In addition, our pull-down data showed that both endoA3 and PSTPIP1 physically interact with the cytosolic tail of L1CAM isoform 1 and 2. Whether these physical interactions are direct or indirect remains to be elucidated. However, a study demonstrated that PSTPIP1 strongly binds to the membrane lipid PI(4,5)P2.[25] This suggests that phosphoinositides could also be involved in the interaction and the recruitment of the F-BAR protein to endocytic sites; this will require further investigations. Interestingly, our TIRF live-cell imaging data demonstrate that endoA3 and PSTPIP1 dynamically co-distribute at the cell surface. Strikingly, the lifetime of the spots for each protein was longer when they co-localised together. This suggests that there is likely a coordination between the two proteins for the stabilisation of the deformation at the plasma membrane. In addition, we observed that PSTPIP1 is systematically recruited 3.32 s before endoA3 to the plasma membrane and leaves the recruitment site 3.14 s after endoA3. This could make sense as PSTPIP1 is a F-BAR domain protein, depicting a much larger intrinsic curvature radius than the N-BAR domain protein endoA3.[4,26] Of note, some F-BAR proteins, like FCHo1 and 2, are known to act as initiators of membrane curvature in CME.[8,9,75] By analogy, a very tempting hypothesis could be that the F-BAR PSTPIP1 intervenes earlier in the CIE process described here to initiate shallow bending of plasma membrane, which would then be further deformed by the N-BAR endoA3.

Given that endoA3 was previously shown to play a role in the uptake of CD166[16] and that L1CAM is part of the same Immunoglobulin-like family, the comparison between the two cargoes is particularly attractive. They are both cell adhesion molecules, presenting similarities in their structures and functions. They are composed of a short cytosolic tail, one transmembrane span and a glycosylated extracellular region containing Ig-like domains.[36] They are expressed in neurons and play an important role in cell adhesion and neuronal development.[39,76] An early study has shown that they even interact together to promote axonal growth.[77] In addition, both CD166 and L1CAM are subject to cleavage of their extracellular part by proteases such as ADAM-10, -17 or MMP-14, -16.[78,79] In the context of cancer, they are both implicated in migration, proliferation and used as tumoral markers.[44,80–82] Finally, their CIE uptake both rely on endoA3, as shown in previous studies[15,16] and demonstrated the current study.

Apart from these commonalities, distinct behaviours between L1CAM and CD166 appear when it comes to the role of glycosylation, galectin binding and glycosphingolipids in their endocytosis. While the uptake of CD166 seems to be driven very specifically by Gal8,[16] the situation is apparently very different for L1CAM in the current study. Although we found Gal1, -3 and -8 in endocytic compartments together with L1CAM, inhibition of galectin binding either led to no change in L1CAM uptake (when specific galectin inhibitors were used), or to an increase in L1CAM uptake (when global galectin binding was inhibited either by LacNAc, in the absence of serum or upon glycosylation perturbation by Kifunensine treatment). A hypothesis could be that galectins—which are able to form a lattice at the cell surface[83]—sequester L1CAM. A refined version of this hypothesis could be that two L1CAM populations exist at the cell surface—one being "free" and another one "trapped" in galectin lattices—in equilibrium (Figure 7). The free L1CAM would require very low local doses of galectins (nanomolar) to drive endocytosis, while L1CAM trapped in lattices would be the consequence of much higher local concentrations of galectins (micro- or millimolar), which would have an inhibitory effect on endocytosis. Accordingly, the study of CD44[84] and CD166[16] uptake demonstrated that only nanomolar doses of galectins

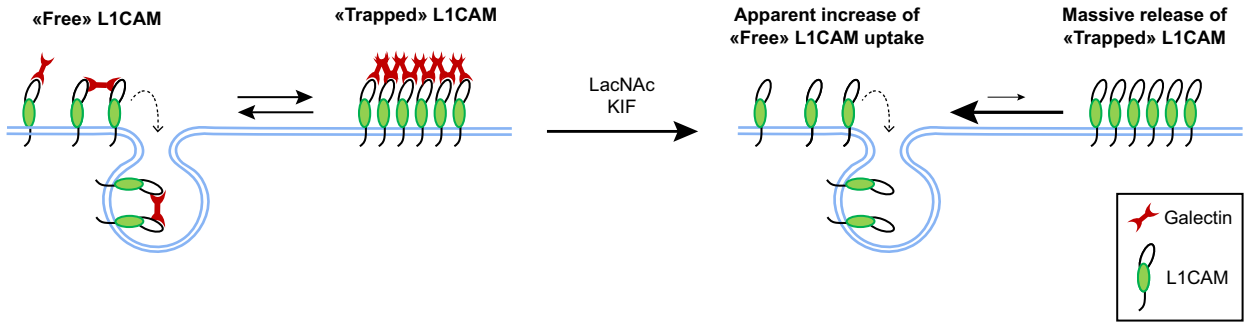

FIGURE 7 Equilibrium between "free" L1CAM and "trapped" L1CAM population. Schematic representation of the hypothesis that galectins sequester L1CAM. Two L1CAM populations exist in equilibrium at the cell surface: one being "free" and another one "trapped" in galectin lattices. The balance is broken after LacNAc or Kifunensine (KIF) treatment, leading to the release of massive amounts of free L1CAM, available for endocytosis. In this situation, even if L1CAM uptake would be driven by galectins, this massive release of L1CAM from lattices would completely hide this phenomenon, leading to an apparent global increase of L1CAM uptake.

are sufficient to drive cargo endocytosis. On the contrary, micromolar doses of galectin-3 resulted in inhibition of CD44 uptake.[84] Similarly, Nabi and Dennis showed that the internalisation of TGF-β and EGFR receptors was blocked because of galectin lattices.[85,86] As proposed by Mathew and Donaldson,[87,88] endocytosis of a cargo is thus dependent on the strength of galectin-glycan interactions: it can be initiated by low amounts of galectins which trigger pit formation, or on the contrary, the cargo can be sequestered at the cell surface due to the formation of lattices by high galectin concentrations. These two extreme situations are part of a continuum between endocytosis and sequestration. Coming back to L1CAM, a global disruption of galectin lattices (with LacNAc treatment, for instance) could thus dramatically modify the equilibrium between "free" and "trapped" L1CAM populations, leading to the release of massive amounts of free L1CAM, available for endocytosis. In this situation, even if L1CAM uptake would be driven by galectins, this massive release of L1CAM from lattices would completely hide this phenomenon, leading to an apparent global increase of L1CAM uptake, even in the absence of galectins.

Unfortunately, the results obtained with specific galectin inhibitors did not allow us to identify the galectins responsible for L1CAM uptake or sequestration at the cell surface. A likely hypothesis could be that inhibition of a single galectin is not sufficient to impact L1CAM endocytosis, probably due to compensation phenomena by other galectins. Even upon combination of inhibitors against Gal1, -3 and -8, other galectins could take over, as many more galectins are expressed[89] or present in the serum. The complex role of galectins and glycosylations in L1CAM endocytosis will require further investigations.

In addition, the uptake of L1CAM remained unaffected when the glycosphingolipid synthesis was inhibited using Genz compound. These results, in combination with the previous data on galectins, suggest that the CIE of L1CAM does not seem to follow the GL-Lect hypothesis.[56] In comparison, the endocytosis of several cargoes such as CD44,[56,84] β1-integrin[56,90] and CD166[16] was strongly reduced by glycosphingolipid depletion and by galectin inhibition. However, given that a significant fraction of L1CAM can be taken up by CME, the possibility exists that compensatory endocytic mechanisms may take over and thwart the effect of Genz. Re-routing of L1CAM via micropinocytosis might be another possibility, as observed previously for CD166,[15] but this remains to be explored.

What may explain the apparent differences between L1CAM and CD166 in terms of endocytic behaviour? L1CAM possesses a larger extracellular domain—1120 amino acids[37]—as compared with CD166—500 amino acids.[91] The number of glycosylation sites is also higher for L1CAM (22)[36] than for CD166 (10).[91] This may completely change the galectin-binding pattern of the two proteins, their interaction with galectin lattice and consequently their endocytic behaviour. Globally, this is valid for every protein, but also for every different cellular context, where glycosylation patterns of the same protein and galectin expression patterns may totally differ, such as in some cancers. Further investigations will be necessary to characterise more thoroughly the molecular mechanism of L1CAM endocytosis via endoA3-mediated CIE in various cellular contexts and establish if molecular determinants are shared with or distinct from CD166 cargo. Additional studies will also be necessary to better grasp the compensation and regulatory mechanisms of multiple endocytic routes.

Moreover, very few publications have addressed the distinction between the two isoforms in pathological contexts. In cancers, both isoforms are co-expressed, but the isoform 2 is generally more abundant.[92,93] In breast cancer cells, both promote motility.[92] However, in ovarian cancer, colorectal cancer, fibrosarcoma and T-cell lymphoma, only the isoform 1 is responsible for metastasis.[93] Thus, deciphering the endocytic process of each isoform will contribute to a better understanding of how their regulation and localisation in cells impact their functions.

To conclude, our study sheds light on a new cargo of endoA3-mediated CIE and will contribute to the better understanding of the physiological relevance of this mechanism in the future.

4 | MATERIALS AND METHODS

4.1 | Cell culture

HeLa (human cervix adenocarcinoma, ATCC CCL-2), and genome-edited U2OS CLTA-mRFP were grown in DMEM high glucose

GlutaMAX Supplement (Gibco, 61965059) supplemented with 10% FBS (Sigma, F7524), 100 U ml^{-1} penicillin and 100 μg ml^{-1} streptomycin (Pen Strep, Gibco, 15140122) and 1 mM pyruvate (Gibco, 110360070). Genome-edited U2OS cells expressing endogenous levels of clathrin light chain (CLTA) tagged with mRFP were a gift from David Durbin's laboratory and were sorted for homogenous expression using FACS. HeLa cells stably expressing GFP-FKBP-tagged endophilin-A3 were generated in our lab[16] and grown in the same medium as the mother cell line, supplemented with 0.125 mg ml^{-1} G418 (Roche, 04727879001). HeLa cells stably expressing L1CAM (isoform 1) tagged with GFP were generated for this study (see below) and grown in the same medium as the mother cell line, supplemented with 0.125 mg ml^{-1} Hygromycin B (Invitrogen, 10687010).

4.2 | Antibodies

The following antibodies were used for immunofluorescence: mouse monoclonal anti-L1CAM clone L1-OV198.5 (BioLegend, 371 602, 1:200, 2.5 μg ml^{-1}); mouse monoclonal anti-clathrin heavy chain antibody clone X22 (gift from E. Smythe, 1:50); anti-mouse conjugated secondary antibodies Alexa Fluor 488 (Invitrogen, A32723, 1:250), Alexa Fluor 546 (Invitrogen, A11030 or A21133, 1:250), or Alexa Fluor 647 (Invitrogen, A21236 or A21240, 1:250).

The following antibodies were used for western-blot analysis: rabbit monoclonal anti-L1CAM clone D5N9S (Cell Signalling Technology, 89 861, 1:1000); mouse monoclonal anti-clathrin heavy chain clone 23 (BD Biosciences, 610 500, 1:5000); mouse monoclonal anti-dynamin clone 41 (BD Biosciences, 610 245, 1:4000); mouse monoclonal anti-α-tubulin clone B-5-1-2 (Sigma, T5168, 1:5000); rabbit monoclonal anti-ezrin clone 2086 (R&D Systems, MAB72391, 1:1000); rabbit polyclonal anti-endoA3 (Sigma Life Sciences, HPA039381, 1:1000); rabbit polyclonal anti-GFP (ChromoTek, PABG1, 1:1000); anti-mouse secondary antibodies conjugated to horseradish peroxidase (Sigma, AP308P); anti-rabbit secondary antibodies conjugated to horseradish peroxidase (Dako, P0448012).

4.3 | Other reagents

Cholera Toxin Subunit B (Recombinant), Alexa Fluor 488 Conjugate (CTxB-A488) was purchased from ThermoFisher Scientific (Invitrogen, C34775). Transferrin From Human Serum, Alexa Fluor 488 Conjugate was purchased from ThermoFisher Scientific (Invitrogen, T13342). Human transferrin-biotin labelled was purchased from Sigma (T3915, 1:500). Streptavidin, Alexa Fluor™ 647 conjugate was purchased from ThermoFisher Scientific (Invitrogen, S21374, 1:200). Genz-123 346 free base compound was purchased from MedChemExpress (HY-12744). GB1107 and GB1490 were kindly synthesised and provided by Galecto Biotech (Lund, Sweden). **19a**[60] and **10b**[61] were kindly synthesised and provided by Mujtaba Hassan and Ulf Nilsson (Lund University, Sweden). K_d values of these inhibitors are available in Supplementary Table 1. N-Acetyl-D-lactosamine (LacNAc) was purchased from Carbosynth (OA08244). Kifunensine was purchased from Biosynth (MK10316). Neuraminidase (Sialidase) was purchased from Roche (10269611001). Endo H_f was purchased from New England Biolabs (P0703S). PFA (Paraformaldehyde 16%) was purchase from Electron Microscopy Sciences (15710) diluted in PBS to obtain 4% concentration. PBS (Phosphate Buffered Saline), BSA (Bovine Serum Albumine) and saponin were purchased from Sigma (D5652-50L, A9647, 47 036, respectively).

4.4 | Recombinant protein production

Recombinant wild-type STxB were purified exactly as mentioned in Reference 16.

Galectins were also cloned and purified as mentioned in Reference 16. In short: All galectins used in this study—Gal3-His, Gal1-His and His-Gal8 in pHis-Parallel 2—were expressed at 20°C overnight in Rossetta2-pLysS E. coli (Novagen) in LB media, supplemented with 60 μM IPTG. Bacterial pellets were resuspended and sonicated in: PBS pH 7.3 for Gal3; PBS pH 7.3, 10% glycerol, 5 mM β-Mercaptoethanol for Gal1; 25 mM HEPES pH 7.3, 300 mM NaCl, 10 mM imidazole, 10% glycerol for Gal8. The Gal8 lysate was adjusted to 5% (w/v) ELUGENT (Merck), kept agitating for 30 min at 4°C. All lysates were cleared by centrifugation at 75000×*g* for 1 h. 95% purity by Coomassie staining was achieved using Cobalt-resin (Pierce) affinity chromatography. Cobalt-resin was washed with resuspension buffer containing 10 mM imidazole for Gal1 and Gal3, and resuspension buffer containing 1% ELUGENT for Gal8. Elution was performed with the following buffers: resuspension buffer containing 300 mM imidazole for Gal1 and Gal3; resuspension buffer containing 20 mM trehalose, 0.2% (w/v) PEG8000 and 300 mM imidazole for Gal8. Gel filtration (HiLoad Superdex 75 16/600) was performed in elution buffer without imidazole. Galectin aliquots were snap frozen in liquid nitrogen and stored at −80°C.

4.5 | Recombinant protein and antibody labelling

For lattice light-sheet microscopy (LLSM), anti-L1CAM antibody or Transferrin were labelled with Alexa647 NHS-ester dye (ThermoFisher Scientific) and Att647N NHS-ester dye (ATTO-TEC GmbH), according to manufacturers' recommendations. Briefly, the protein was labelled in Hepes buffer at pH 8.0 using a 4- to 5-fold molar excess of dye (resuspended and conserved in anhydrous DMSO). The reaction mix was protected from light and incubated for 3 h at 16°C under mild agitation. Free dye was then removed by gel filtration on two to three PD SpinTrap G-25 columns (GE Healthcare), and the labelled protein was recovered in PBS. Galectins were coupled to mono-amine-reactive (NHS-ester) Cy3, Cy5 (GE Healthcare) or Alexa-488 in final purification buffer supplemented with 10 mM lactose for 3 h at 16°C, using a molar ratio of 1:4 (protein/dye). The mixture was purified in the same buffer without lactose

and a PD-10 column (GE Healthcare). Labelling efficiency was 0.9 (Gal1), 1.1 (Gal3) and 0.96 (Gal8-N-CRD), and 1.2 (Gal8).

4.6 | siRNA transfection

Cells were transfected with a mix containing Opti-Mem (Gibco, 31985062), siRNA at a final concentration of 40 nM, and HiPerFect (Qiagen, 301705). Experiments were performed 72 h after transfection. All siRNAs were purchased from Qiagen. siCtrl (AllStars Negative Control siRNA, 1 027 281) served as a reference point. The depletion of μ2-adaptin was achieved with one sequence: SI02777355 (5′-TGCCATCGTGTGGAAGATCAA-3′). The depletion of endophilin-A1, endophilin-A2, endophilin-A3, PSTPIP1 and endogenous L1CAM (L1CAMe) was achieved with two different sequences pooled: siEndoA1 #1 (SI04149411: 5′-AAAGACTCTTTGGACATAGAA-3′), siEndoA1 #2 (SI04260949: 5′-AAATCTGGTATCCAAGCTTAA-3′), siEndoA2 #1 (SI03057250: 5′-CACCAGCAAGGCGGTGACAGA-3′), siEndoA2 #2 (SI03073931: 5′-CATGCTCAACACGGTGTCCAA-3′), siEndoA3 #1 (SI04170376: 5′-CCAGACGAGAATACAAGCCAA-3′), siEndoA3 #2 (SI04176529: 5′-CCAGACGAAGAAGTCAGACAA-3′), siPSTPIP1 #1 (SI00058576: 5′- ACCGGGCGCTCTACGATTATA-3′), siPSTPIP1 #2 (SI00058583: 5′-CAGCATAGACGCCGACATCGA-3′), siL1CAMe #1 (SI05051277: 5′-TAGGTGGTTTCTAGGATTGAT-3′) siL1CAMe #2 (SI05051284: 5′-TGGCTGGGACTGGGAACAGAA-3′). For uptake rescue experiment (Figure 3C), two specific sequences against endoA3 were used in order to allow transient expression: siEndoA3 #1 (SI05081167: 5′-TACCTGTGAATAGCCCAATAA-3′) and siEndoA3 #2 (SI05081174: 5′-TACTTTCGTAACTGAAATGAA-3′). The depletion of clathrin heavy chain and dynamin-2 and was achieved with a smartpool of four sequences: siCLTC (SI00299873: 5′-AAGGAGAGTCTCA GCCAGTGA-3′; SI00299880: 5′-TAATCCAATTCGAAGACCAAT-3′; SI04152372: 5′-AAGGGCTAACGTCCCAAATAA-3′; SI04190417: 5′-CCCTGAGTGGTTAGTCAACTA-3′), siDNM2 (SI02654687: 5′-CTGCAG CTCATCTTCTCAAAA-3′; SI03233671: 5′-TCGCAACCTGGTGGACT-CATA-3′; SI04224591: 5′-CTCATACGTGGCCATCATCAA-3′; SI04277 546: 5′-CCCGCTGGTCAACAAACTGCA-3′).

4.7 | Plasmid transfection and DNA constructs

For plasmid transfection, cells were transfected with a mix containing Opti-Mem (Gibco, 31985062), plasmid and FuGene HD (Promega, E2311). Experiments were performed 16-24 h after transfection. mCherry-tagged μ2 subunit of AP-2 and GFP-tagged PSTPIP1 were kindly provided by C. Merrifield and D. Gumucio, respectively. The GFP and mCherry-tagged human endoA3 constructs were previously engineered in the lab.[16] The expression plasmid pEGFP-N1 (free-GFP) was purchased from Clontech.

For this study, two L1CAM constructs were engineered: human L1CAM-iso1 fused to GFP and human L1CAM-ΔRSLE (lacking amino acids 1177 to 1180) fused to mCherry. For L1CAM-iso1 fused to GFP, we first amplified GFP by PCR from the expression plasmid pEGFP-N1 (forward primer with BamHI restriction site: 5′-CGCGGATCCATGGTGAGCAAGGGC-3′; reverse primer with BstXI restriction site: 5′- ATGCATCCAGCACACTGGTTACTTGTACAGCTC-3′) and cloned the fragment obtained into the bicistronic vector pIRE-Shyg3 (Clontech) between BamHI and BstXI restriction sites. Then, L1CAM-ΔRSLE was incorporated into pIREShyg3-GFP thanks to the Gibson Assembly method. Using PCR, we then amplified L1CAM-ΔRSLE from the expression plasmid pcDNA3-hL1 (Gift from Fritz - Rathjen, Addgene plasmid # 89411) (forward primer: 5′- GGATCTGTA-CAGGCCTTAAGATGGTCGTGGCGCTGCGGTA-3′; reverse primer: 5′-TCACCATGGATCCGAATTCGCCTTCTAGGGCCACGGCAGG −3′) and pIREShyg3-GFP (forward primer: 5′-ACCCTGCCGTGGCCCTAGAAGG CGCGCTAGCGCTTCGAAG ACCCTGCCGTGGCCCTAGAAGGCGCG CTAGCGCTTCGAAG-3′; reverse primer: 5′- TACCGCAGCGCCAC-GACCATCTTAAGGCCTGTACAGATCC -3′). The assembly of PCR fragments was performed according to the manufacturer's instructions (Gibson Assembly Master Mix, New England Biolabs, E2611S). Finally, in order to obtain the full-length version of L1CAM, the insertion of the 12 nucleotides coding for the exon 27 (RSLE) was achieved with the Q5 Site-Directed Mutagenesis Kit (New England Biolabs, E0554S) according to the manufacturer's instructions (forward primer: 5′-CTGGAGAGTGACAACGAGGAGAAGGC-3′; reverse primer: 5′-GGACCTGTACTCGCCGAAGGTCTCAT-3′). For L1CAM-ΔRSLE fused to mCherry, we first amplified mCherry sequence by PCR from the expression plasmid pmCherry-N1 (Clontech) (forward primer with BamHI restriction site: 5′-CGCGGATCCATGGTGAGCAAGGGC-3′; reverse primer with NotI restriction site: 5′-TTTTCCTTTTGCGGCCG CCTACTTGTACAGCTC-3′) and cloned the fragment obtained into the bicistronic vector pIRESpuro3 (Clonetch) between BamHI and NotI restriction sites. Then, L1CAM-ΔRSLE was incorporated into pIRESpuro3-mCherry thanks to the Gibson Assembly method. Using PCR, we amplified L1CAM-ΔRSLE from the expression plasmid pcDNA3-hL1 (forward primer: 5′-CGGCCTAGCTAGCGCTTAAGATGG TCGTGGCGCTG CGGTA-3′; reverse primer: 5′-TCACCATGGATCC-GAATTCGCCTTCTAGGGCCACGGCAGG-3′) and pIRESpuro3-mCherry (forward primer: 5′-CCTGCCGTGGCCCTAGAAGGCGAATTC GGAT CCATGGTGA-3′; reverse primer: 5′-TACCGCAGCGCCACGAC-CATCTTAAGCGCTAGCTAGGCCG-3′). The assembly of PCR fragments was performed according to the manufacturer's instructions of the Gibson Assembly Master Mix. At each step, correct clones were validated by sequencing.

For pull-down assays, two GST-tagged constructs were generated: the cytoplasmic tails of L1CAM isoform 1 (GST-iso1) and isoform 2 (GST-iso2). The cytoplasmic tail of L1CAM isoform 1 was amplified by PCR from the expression plasmid pIREShyg3-L1CAM-iso1-GFP (see above), and the cytoplasmic tail of L1CAM isoform 2 from the expression plasmid pcDNA3-hL1 (forward primer with EcoRI restriction site: 5′-CCGGAATTCAAGCGCAGCAAGGGCGGCAA-3′; reverse primer with XhoI restriction site: 5′-CCGCTCGAGCTATTCTAGGGCCACGGCA-3′). To obtain the final constructs, the amplified L1CAM tail sequences were inserted into the expression plasmid pGEX-4T1 (GE Healthcare) encoding for GST between EcoRI and XhoI restriction sites. Correct clones were validated by sequencing.

To generate HeLa cells stably expressing L1CAM-iso1-GFP, pIREShyg3-L1CAM-iso1-GFP expression plasmid was transfected by nucleofection (Lonza, Amaxa Cell Line Nucleofector Kit R, VCA-1001) and selection was carried out with 0.25 mg ml^{-1} Hygromycin B for 10 days. Surviving colonies were harvested and grown individually. The selection pressure was decreased to 0.125 mg ml^{-1} Hygromycin B for further culture. Only the fluorescent colonies were conserved.

4.8 | Flow cytometry

The flow cytometer Guava easyCyte (Merck-Millipore) was used for the measurements of loss-of-surface assay (Figures 1A, B, 3B and 4A), of protein surface level, of galectin binding (Figure S6A, C, E, G) and of continuous uptake of galectins (Figure S6B, D, F, H). 10 000 cells were counted per condition and median fluorescence intensity was measured.

4.9 | Loss-of-surface assay

The loss-of-surface assays of anti-L1CAM and transferrin (Figures 1A, B, 3B and 4A) were performed as described previously.[16] Briefly, transfected cells were pre-incubated in DMEM containing 25 mM HEPES (Gibco, 32 430 027) and 10% FBS for 30 min at 37°C under 5% CO_2. For transferrin, cells were pre-incubated in the same medium without FBS (and no FBS was added to the culture medium for the rest of the experiment). Then, plates were transferred on ice and washed with ice-cold culture medium. Cells were incubated with ice-cold culture medium with anti-L1CAM (2.5 μg ml^{-1}) or transferrin-biotin (1:500) for 30 min on ice. After several washes, pre-warmed culture medium was added on the cells, and they were put back to 37°C under 5% CO_2 for different times to launch endocytosis. One plate was kept on ice to provide the cell surface level of the cargoes, corresponding to the 0 min time point (0% endocytosis). Cells were put on ice again to stop endocytosis, washed with ice-cold PBS++ (PBS supplemented with 0.4 mM $MgCl_2$ and 0.9 mM $CaCl_2$) with 0.2% BSA and incubated in the same solution for 15 min. The remaining anti-L1CAM at the cell surface was then labelled with fluorescent secondary antibodies Alexa Fluor 488 or 647 (1:250) during 30 min in ice-cold PBS++ with 0.2% BSA. The remaining transferrin-biotin at the cell surface was labelled with the fluorescent streptavidin Alexa Fluor 647 (1:250) in the same conditions. Cells were then washed several times, and finally detached by an incubation of 45 min in ice-cold PBS with EDTA 4 mM. Cell suspensions were kept on ice until measurements by flow cytometry. The percentage of endocytosis at each time point was derived from the fraction of the remaining cell surface signal reported to the total surface signal at time 0.

4.10 | Surface level measurement

For uptake experiments on transfected cells (Figures 1C, 3A, C, 4B, C, 5F, H and S4B) or on cells treated with Genz or Kifunensine (Figures 6H and S7D, E) surface level measurements of L1CAM were performed in order to correct the total uptake of the cargo measured per cell (see the "Quantification of cargo uptake from confocal images" section). Briefly, cells were pre-incubated in DMEM supplemented with 25 mM HEPES and 10% FBS for 30 min at 37°C under 5% CO_2. Then, plates were transferred on ice and washed with ice-cold PBS++ containing 0.2% BSA, and incubated for 15 min in this solution. Cells were then incubated with ice-cold PBS++/0.2% BSA containing anti-L1CAM (2.5 μg ml^{-1}) for 30 min on ice. After several washings, cells were incubated in ice-cold PBS++/0.2% BSA with secondary antibodies conjugated to Alexa Fluor 488 or 647 (1:250). Cells were washed again, and finally detached after an incubation of 45 min in ice-cold EDTA 4 mM. Cell suspensions were kept on ice until analysis by flow cytometry. For the measurements of efficacy and specificity of the galectin inhibitors at 4°C (Figure S6A, C, E, G), the protocol is similar except that cells were first incubated for 30 min at 37°C under 5% CO_2 in pre-warmed Lactose Buffer (150 mM lactose, 20 mM HEPES, 45 mM NaCl, 5 mM KCl, 1 mM $MgCl_2$, 1 mM CaCl2, pH 7.2) to compete any present galectins. Then, for the labelling step, cells were incubated in ice-cold PBS++/0.2% BSA with the inhibitors at the specified concentration and the fluorescent galectins (50 nM Gal1-Cy5, 200 nM Gal3-A488, 50 nM Gal8-Cy5, 50 nM Gal8-N-CRD-Cy5), for 1 h on ice.

4.11 | Continuous uptake in flow cytometry

For the measurements of efficacy and specificity of the galectin inhibitors at 37°C (Figure S6B, D, F, H), the inhibitors at the specified concentration and the fluorescent galectins (50 nM Gal1-Cy5, 200 nM Gal3-A488, 50 nM Gal8-Cy5, 50 nM Gal8-N-CRD-Cy5) were first incubated in DMEM supplemented with 25 mM HEPES at 37°C for 10 min. Then, the mix was incubated on cells for 30 min at 37°C, 5% CO_2. Next, plates were transferred on ice to directly go to the final cell detachment step.

4.12 | Light microscopy

For immunofluorescence studies, cells were fixed in 4% PFA at 37 °C for 15 min (Figures 2A, B, 3D, 4D, 5D, E and S2) or for 10 min at 4°C followed by an additional 10 min at room temperature (Figures 1C, 3A, C, 4B, C, 5F–H, 6A–C, 6E–H, S4B and S7A–E). All other subsequent steps were performed at room temperature. PFA was quenched with 50 mM NH_4Cl for 15 min. Cells were then permeabilised with a solution of 0.02% saponin and 0.2% BSA in PBS for 30 min, and incubated with primary or secondary antibodies diluted in the same solution for 40 min. Samples were mounted with Fluoromount-G (Invitrogen, 00-4958-02). Fixed samples were imaged with a Zeiss LSM 710 confocal microscope equipped with an Airyscan 34-channel detector and with a Plan Apo 63× numerical aperture (NA) 1.4 oil immersion objective.

For live-cell imaging (Figures 3E, 4E–I, S3, S5 and Movies S5–S9), cells were grown to sub-confluence on 24-well SensoPlate glass bottom (Greiner bio-one, 662892) and observed at 37 °C under 5% CO_2.

Live-cell confocal images were acquired on the previously described Zeiss LSM710 microscope. Live-cell TIRF images were acquired on a Zeiss Axio Observer 7 microscope equipped with an iLas azimuthal TIRF module (Gattaca Systems), an α Plan-Apo 100× NA 1.46 oil immersion objective and an sCMOS Prime BSI Express camera (Photometrics). Montages, kymographs and movies were prepared with Fiji software (NIH).

4.13 | Uptake assays

4.13.1 | Anti-L1CAM antibody uptake in siRNA-transfected cells

The uptake assays of anti-L1CAM antibodies in cells transfected with specified siRNA (Figures 1C, 3A, C, 4B, C, 5F, H and S4B) were performed as described previously.[16] In order to reach sub-confluence on the day of the experiment, cells were seeded in 4-well plates 16-24 h before the experiment. Briefly, transfected cells were pre-incubated in DMEM supplemented with 25 mM HEPES and 10% FBS for 30 min at 37°C, 5% CO_2. Cells were then incubated in pre-warmed culture medium containing anti-L1CAM antibody (2.5 μg ml^{-1}) for 10 or 30 min at 37°C, 5% CO_2. Next, plates were transferred on ice and washed with ice-cold PBS++ to stop intracellular trafficking processes. The remaining antibodies at the cell surface were removed by three 20-s ice-cold acid washes (300 mM NaCl, 5 mM KCl, 1 mM $CaCl_2$, 1 mM $MgCl_2$, 0.2 M acetic acid, pH 2.5). Cells were quickly and repeatedly washed with ice-cold PBS++. Then, cells were fixed, permeabilised, incubated with the secondary antibodies, and mounted as described in "Light microscopy" section.

4.13.2 | Anti-L1CAM antibody uptake in cells treated with inhibitors

For these experiments, the protocol is similar but with various pre-incubations:

- Galectins inhibitors (Figure 6G): Inhibitors solubilised in DMSO (GB1107 and GB1490: 3 μM; **19a** and **10b**: 50 μM) were first incubated in culture medium supplemented with FBS at 37°C for 10 min. Then, the inhibitor mix was put on the cells for 30 min at 37°C under 5% CO_2. Next, anti-L1CAM antibody (2.5 μg ml^{-1}) was added to each well for an additional 10 min.
- Glycosphingolipid depletion (Figure 6H): Cells were pre-treated for 48 h with 5 μM Genz-123 346.
- 10 mM LacNAc (Figure 6E): Cells were pre-incubated in serum-free culture medium with 10 mM LacNAc for 5 min at 37°C under 5% CO_2. Then, cells were incubated in the same culture medium containing anti-L1CAM antibody (2.5 μg ml^{-1}) with or without 10% FBS, or with 10 mM LacNAc, for 10 min at 37°C under 5% CO_2.
- Neuraminidase treatment (Figure S7C): Cells were pre-incubated in serum-free culture medium supplemented with Neuraminidase (1:100, 35 mU per well) for 2 h30 at 37°C under 5% CO_2.
- Mannosidase inhibition (Figure S7D, E): cells were pre-treated for 48 h with 2 μg ml^{-1} Kifunensine. For Figure S7D, cells were pre-incubated in DMEM supplemented with 25 mM HEPES and 10% FBS for 30 min at 37°C, 5% CO_2. For Figure S7E, cells were pre-incubated serum-free culture medium supplemented with 10 mM LacNAc for 30 min at 37°C under 5% CO_2. Then, cells were incubated in pre-warmed culture medium with anti-L1CAM antibody (2.5 μg ml^{-1}), with or without 10% FBS, for 10 min at 37°C, 5% CO_2.

4.13.3 | Galectin uptake

For the uptake of Gal3-A488 and Gal8-Cy3 (Figure S7B), cells were first treated with Neuraminidase for 2h30 (see above). Then, cells were incubated in DMEM supplemented with 25 mM HEPES and 50 nM Gal3-A488 or 50 nM Gal8-Cy3 for 10 min at 37°C under 5% CO_2. Next, plates were transferred on ice and washed with ice-cold PBS++ to intracellular trafficking processes. The remaining galectins on the cell surface were removed by three 5-min ice-cold Lactose Buffer washes (150 mM lactose, 20 mM HEPES, 45 mM NaCl, 5 mM KCl, 1 mM $MgCl_2$, 1 mM $CaCl_2$, pH 7.2). Cells were quickly washed again with ice-cold PBS++. Then, cells were fixed and mounted as described in "Light microscopy" section.

4.13.4 | Co-uptake of anti-L1CAM antibody and galectins

The binding of ligands to the cell surface was performed sequentially—galectins first, antibody second—as galectins are susceptible to bind to glycosylations of antibodies, creating biased co-localisation (Figure 6A–C). Briefly, cells were first pre-incubated in Lactose Buffer for 30 min at 37°C, 5% CO_2. Next, plates were transferred on ice, washed with ice-cold PBS++ and incubated in ice-cold DMEM supplemented with 25 mM HEPES and a galectin (50 nM Gal1-Cy5, 200 nM Gal3-A488 or 50 nM Gal8-Cy3) for 20 min. Then, cells were washed again with ice-cold PBS++, incubated in ice-cold culture medium containing anti-L1CAM antibody (2.5 μg ml^{-1}) for 20 min, and washed a third time. Afterwards, cells were switched to 37°C in pre-warmed culture medium for 10 min, to launch endocytosis. Plates were then placed back on ice, washed first with ice-cold PBS++, followed by three 5-min ice-cold Lactose Buffer washes and three 20-s ice-cold acid washes. Ice-cold PBS++ washes were performed before and after each wash. Then, cells were fixed, permeabilised, incubated with the secondary antibodies and mounted as described in "Light microscopy" section.

4.13.5 | Continuous uptake in immunofluorescence

Cells were seeded in 4-well plates 16-24 h in advance to reach sub-confluence on the day of the experiment. On the day of experiment, for continuous uptake of anti-L1CAM antibody (Figures 3D, 4D and 5E), cells were pre-incubated in culture medium

supplemented with FBS, for 30 min at 37°C, 5% CO_2. Then, cells were incubated for 5 or 10 min in culture medium with anti-L1CAM antibody (2.5 μg ml^{-1}). For continuous uptake of transferrin and anti-L1CAM antibody over time (Figure 2A, B), cells were first placed on ice and washed with ice-cold PBS++. Then, they were incubated with transferrin-A488 (10 μg ml^{-1}) or anti-L1CAM antibody (2.5 μg ml^{-1}) in ice-cold PBS++ for 30 min, followed by several washes with ice-cold PBS++. Afterwards, cells were switched to 37°C, 5% CO_2 in pre-warmed PBS ++ for various times, to launch endocytosis. Finally, for all experiments, cells were fixed, permeabilised, incubated with the secondary antibodies and mounted as described in "Light microscopy" section.

4.13.6 | STxB binding

To measure the efficiency of Genz-122 346 (Figure S7A), STxB binding at the cell surface was achieved by confocal microscopy. First, cells were pre-treated for 48 h with 5 μM Genz-123 346. Then, cells were directly incubated in pre-warmed DMEM supplemented with 25 mM HEPES, 10% FBS and 200 nM STxB-A488 for 10 min at 37°C, 5% CO_2. Then, cells were fixed, permeabilised, incubated with the secondary antibodies and mounted as described in "Light microscopy" section.

4.14 | STxB and CTxB-induced plasma membrane tubulation

These experiments (Figure S2) were performed as previously described.[11] Briefly, cells were pre-incubated for 15 min at 37°C, 5% CO_2 in ATP depletion medium, composed of PBS++ supplemented with 10 mM 2-deoxy-D-glucose (Sigma, D8375) and 10 mM NaN_3. Then, cells were incubated in the same pre-warmed medium supplemented with 200 nM STxB-Cy3 or 0.2 μg ml^{-1} CTxB-A488 for 15 min at 37°C, 5% CO_2. Finally, cells were fixed and permeabilised, L1CAM was detected by immunofluorescence and samples were mounted as described in "Light microscopy" section.

4.15 | Live-cell lattice light-sheet microscopy

The experiment (Figure 2E–G and Movies S1–S4) was performed in genome-edited U2OS cells expressing endogenous levels of clathrin light chain (CLTA) tagged with mRFP. The endocytosis experiments of fluorescent anti-L1CAM antibody or transferrin were performed as previously established with minor modifications.[16] In brief, U2OS-CLTA-mRFP cells were plated 6 h before imaging on 5 mm #1.5 coverglass (Electron Microscopy Sciences, cat#72195-05). Media was changed to CO_2-independent lattice light-sheet (LLS) imaging media (phenol-red free DMEM, high glucose, glutamax, supplemented with sterile 1% BSA, 0.01% penicillin and streptomycin, 1 mM pyruvate and 20 mM HEPES [pH 7.3]). Cells were incubated for 2 min with anti-L1CAM-Alexa647 antibody (90 nM, Biolegend, clone L1-OV198.5, labelling efficiency 3.5) or with transferrin-Atto647N (50 nM, labelling efficiency 4) diluted in LLS-imaging media at 21°C. The coverslips were transferred into the imaging chamber containing LLS-imaging media at 30 °C (for increased stability of the optical system). 4D acquisition started within 2–3 min using a commercial LLS-microscope of 3i (Denver, USA), as previously described.[94] Cells were scanned incrementally with a 20 μm long light sheet in 600 nm steps using a fast piezoelectric flexure stage equivalent to ~325 nm with respect to the detection objective and were imaged using two sCMOS cameras (Orca-Flash 4.0; Hamamatsu, Bridgewater, NJ). Excitation was achieved with a 560 or 642 nm diode lasers (MPB Communications) at 10 acousto-optic tunable filter transmittance with 100 mW initial box power through an excitation objective (Special Optics 28.6× 0.7 NA 3.74 mm water-dipping lens) and detected via a Nikon CFI Apo LWD 25× 1.1 NA water-dipping objective with a 2.5× tube lens. LLS imaging was performed using an excitation pattern of outer NA equal to 0.55 and inner NA equal to 0.493. A composite volumetric dataset of 60 slices per cell was acquired within 3 s using 20 ms exposure per slice and channel. 50 time points were acquired per cell. Raw images of obtained datasets were quantitative analysed using an adapted version of cmeAnalysis3D software published previously[16,95] and as described in the "Quantitative analysis and visualisation of live cell lattice light-sheet dataset" section.

4.16 | Pull-down assays

Pull-down (Figure 5A, B) were performed as described in Reference 16 with slight modifications. Briefly, 2 L of BL-21 Escherichia coli were transformed with GST-iso1, GST-iso2 and GST constructs (see "Plasmid transfection and DNA constructs" section). Protein synthesis was induced with 100 μM IPTG (Sigma, 16758) for 3 h at 30°C. From here, each step was done at 4°C or on ice. Cell cultures were centrifuged at 8000×*g*, the pellets were washed with water, centrifuged again at 8000×*g* and finally the pellets were resuspended in a lysis buffer composed of 150 mM NaCl, 25 mM HEPES, pH 7.4 and 2 mM EDTA complemented with 1 mM PMSF, 2 mM DTT, 100 μg ml^{-1} lysozyme (Sigma, 62 970) and protease inhibitor cocktail. Cells were kept on ice for 30 min and lysed by snap-freezing in liquid nitrogen, quick thawing and three 20 s sonications (amplitude 40). Lysates were clarified by ultracentrifugation in a Beckman Ti45 rotor for 30 min at 41000 rpm (~131 000×*g*). The supernatant, containing the proteins, was bound to 2 ml of Glutathione Sepharose resin (GE Healthcare, GE17-5132-01), previously equilibrated with the lysis buffer (150 mM NaCl, 25 mM HEPES, pH 7.4 and 2 mM EDTA), for 1 h under agitation on a tube roller. Resin was washed twice with 20 ml of lysis buffer and twice with 40 ml of wash buffer (500 mM NaCl, 25 mM HEPES, pH 7.4 and 2 mM EDTA). Finally, protein-bound resins were resuspended in 1.5 ml of lysis buffer complemented with 0.02% NaN_3.

HeLa cells stably expressing GFP-tagged endoA3 or transiently expressing PSTPIP1-GFP, were transferred on ice and washed with ice-cold PBS. Cells were lysed with the same lysis buffer used before, complemented with 1 mM PMSF, 1% NP-40, phosphatase inhibitor

cocktail, and protease inhibitor (PhosSTOP, Roche, 04906845001), incubated on ice for 30 min, followed by three 20-s sonications (amplitude 40). Lysates were centrifuged for 15 min at 14000×*g*. The supernatant was exposed to 100 µl of each resin (GST alone, GST-iso1, GST-iso2) for 2 h at 4°C on a rotation wheel. The samples were centrifuged at 500×*g* and washed five times with a washing buffer (200 mM NaCl, 25 mM HEPES, pH 7.4 and 2 mM EDTA complemented with 1% NP-40). The resin was resuspended in sample buffer (62.5 mM Tris–HCl, 2% SDS, 5% glycerol, 2.5% β-Mercaptoethanol, 0.005% blue bromophenol) and heated at 95°C for 10 min for elution. 10 µl of each sample were run on SDS-PAGE ("input" lane corresponds to the total cell lysate diluted 30 times). The proteins were transferred and immunoblotted using anti-ezrin, anti-endoA3, anti-GFP and anti-endoA2 antibodies. In addition, gels were stained with InstantBlue Coomassie (abcam, ab119211) to control the amount of GST fragments in each sample.

4.17 | cDNA production

cDNA production was performed as described in Reference 16 with slight modifications.

4.17.1 | RNA extraction

RNA extraction was performed with TRIzol (Invitrogen, 15596026), according to manufacturer's instructions. Briefly, cells from one confluent flask or 10 cm diameter dish were harvested by trypsinisation, and then centrifuged. The pellet was resuspended in 1 ml of TRIzol and incubated at room temperature for 5 min. 200 µl of chloroform was added in the sample. Then, the sample was mixed by vortexing and centrifuged at 12000×*g* for 15 min at 4°C, to allow phase separation. The upper aqueous phase containing RNA was retrieved. 500 µl of isopropanol was added to the sample. This was incubated for 10 min at room temperature to allow RNA precipitation. Then, the sample was centrifuged at 12000×*g* for 10 min at 4°C. The supernatant was discarded and the pellet obtained was washed in 75% ethanol (v/v). A final centrifugation was performed at 7500×*g* for 5 min at 4°C, the supernatant was discarded, and the sample was air-dried at room temperature for ±10 min. The pellet was resuspended in 25 µl of water and heated at 55°C for 10 min. RNA concentration was measured with a Nanodrop device and adjusted at 500 ng ml^{-1}.

4.17.2 | Reverse transcription

Production of cDNA from RNA was performed with QuantiTect Reverse Transcription Kit (Qiagen, 205 311), according to manufacturer's instructions. Briefly, traces of genomic DNA were first eliminated, followed by reverse transcription for 15 min at 42°C. The reverse transcriptase was inactivated by eating 3 min at 95°C. cDNA was obtained from 1 µg RNA and stored at −20°C.

4.18 | Quantification of gene expression by qPCR

4.18.1 | Primer design

Primers for qPCR were designed using the "NCBI Primer Designing Tool". The protein PSTPIP1 was targeted with two couples of primers (forward primer #1: 5′-GCTTCTGGATGGCAGGAAGA-3′; reverse primer #1: 5′-CGATCTGCACCAGCTCCTTC-3′; forward primer #2: 5′-AGCTGCAGTTCAAAGATGCC-3′; reverse primer #2: 5′-TGCACATCTTCCTGCCATCC-3′). Three genes were chosen as reference: ACTB (forward primer: 5′-CCTCGCCTTTGCCGATCC-3′; reverse primer: 5′-CTCGTCGCCCACATAGGAAT-3′), GAPDH (forward primer: 5′-GGTCACCAGGGCTGCTTTTA-3′; reverse primer: 5′-TTCCCGTTCTCAGCCTTGAC-3′) and 18 s RNA (forward primer: 5′-GGCCCTGTAATTGGAATGAGTC-3′; reverse primer: 5′-CCAAGATCCAACTACGAGCTT-3′).

4.18.2 | qPCR

qPCRs were performed with qPCR Mastermix Plus for SYBR Green (Eurogentec, RT-SN2X-06+) on StepOnePlus (Applied Biosystems) real-time PCR machine. Efficiency of primers was comprised between 90 and 110%.

4.19 | Cell lysates

To obtain cell lysates for western-blot analysis (Figures 1D, 5C, G and S7F), cells were lysed with 50 µl of sample buffer and then heated at 95°C for 10 min. Lysates were conserved at −20°C. For the lysates treated with Endo H_f (Figure S7F), 10 µg of protein lysate was digested with Endo H_f for 1 h at 37°C.

4.20 | Western-blot

For all western-blot (Figures 1D, 5C, G and S7F), 8 µl of prestained protein ladder (Thermo Scientific, 26 617) and 5 to 10 µg of protein lysate were loaded on a Mini-Protean TGX 4%–15% gel, 10 or 15 wells (Biorad, 4 561 084 or 4 561 086). Migration was performed in a TRIS-Glycine buffer for 30 min at 200 V, with a PowerPac machine (Biorad, 1645052). The proteins were transferred with the Trans-Blot Turbo machine (Biorad, 1704150) for 3 min at 2.5A and 25 V, using a Trans-Blot Turbo Transfer Pack (Biorad, 1704156). The membranes were cut according to the size of the proteins of interest. Membranes were saturated in a PBS, Tween 20 0.1% and 5% milk solution for 30 min at room temperature, followed by the primary antibody incubation in the same solution for at least 1 h at room temperature or over-night at 4°C. Membranes were washed three times with PBS, Tween 20 0.1% and then incubated for a least 1 h in secondary antibody solution. Membranes were washed three times and then revealed by chemiluminescence with West Femto (Thermo Scientific, 34095) in an Amersham

Imager 600 machine (GE Healthcare, 29-0834-61). Images were treated and cropped with (Fiji Is Just) ImageJ 2.3.0/1;53t (NIH) software.

4.21 | Image quantifications

All image quantifications were performed with (Fiji Is Just) ImageJ 2.3.0/1;53t (NIH) and Icy v2.4.2.0 (Institut Pasteur) softwares, except for LLSM images. For LLSM image quantifications, please see the "Quantitative analysis and visualisation of live cell lattice light-sheet dataset" section.

4.22 | Quantitative analysis and visualisation of live-cell lattice light-sheet dataset

Post-processing of raw data volumes was carried out as described previously.[95] Automated detection of clathrin-coated structures or punctate structures of fluorescently labelled cargoes (CD171 antibody or transferrin) in 3D was performed by numerical fitting with a model of the microscope point spread function (PSF) as described previously.[95] Automated tracking of cargo and clathrin was calculated using the u-track software package,[96] included in the cmeAnalysis3D software,[95] which was implemented in Matlab 2021b. We used clathrin and cargo detection positions to map the membrane shape using the Matlab function of alphaShape. We then calculated the displacement of each cargo from the plasma membrane position orthogonally into the interior of the cell. The distinction between point-like structures moving inside the plasma membrane and the internalised molecules, whether clathrin-dependent or clathrin-independent, was made using membrane position detection. An event was counted as an endocytic event if an object undergoes a net displacement of at least 150 nm from the initial position inside the membrane proximal zone.[16] The membrane proximal zone was limited by the contour of the alphaShape and a line 400 nm inwards of the cell.[16] To calculate the number of clathrin-dependent and clathrin-independent events, the presence of clathrin was assessed for each qualified internalisation event of the cargo channel using the cmeAnalysis3D software. Only tracks with duration of more than 13.5 s were used for the analysis. The calculation of the lifetime distributions and intensity cohorts were performed as described previously in detail.[95] The raw LLSM images, used in Figure 2F, G and in Movies S1–S4, were deconvolved using LLSpy v0.4.3[97] before video rendering and visualisation using Napari.[98] The analysis code can be found as part of the Github repository of llsmtools in https://github.com/francois-a/llsmtools/.

4.23 | Quantification of cargo uptake from confocal images

Cargo uptake quantification was performed as described previously.[16] Confocal images were quantified using Icy software. Briefly, regions of interest (ROIs) were drawn manually around each cell. Within each cellular ROI, bright spots corresponding to endocytic structures were automatically detected over dark background using the "Spot Detector" plugin. The plugin performs image denoising by computing wavelet adaptive threshold (WAT) on the union of all ROIs present in an image. This automatic thresholding was then manually adjusted, depending on the size of the spots: for each independent experiment, we chose scale 2 and adjusted sensitivity empirically. As an output, we obtained the number of endocytic structures within each cell and their respective intensities, which we summed to obtain the total uptake of the cargo per cell. These uptake values were then corrected with the surface level of the proteins (see the "Surface level measurement" section). For each experiment, data were normalised to the control condition (set as 100%).

4.24 | Quantification of co-localisation

Quantification of co-localisation between two channels was performed using an object-based method with the JACoP plugin[99] in ImageJ software. First, background was substracted using a rolling ball radius of 50 pixels, the outline of the cell was drawn manually and everything outside was cleared in order to have one single cell per image. Then, protein spots were detected by finding maxima in the images using the "find maxima" plugin of ImageJ, whose noise tolerance parameter was set up visually independently for each channel. This generated a map of the spots, and the spots were grown by expansion to 2-pixel radius. Finally, the JACoP plugin was used and measured the co-localisation based on distance between centres of mass. This provided the data for the "specific co-localisation". To measure the "random co-localisation", the spot map of a channel was rotated by 90° to measure co-localisation due to chance. The results were expressed as the percentage of co-localising spots over the total number of spots in one of the two channels.

4.25 | Co-localisation of tracks in TIRF time series

Co-localisation of tracks (Figure 4F) was performed with Fiji 1.53t (NIH) and JMP Pro v16.0 software. Briefly, for each channel, tracks were detected in Fiji thanks to the TrackMate plugin.[100] For spot detection, the radius was set to 0.25 µm and the sensitivity threshold was adjusted depending on protein expression levels. The tracking was done with the LAP tracker with a maximum distance between two spots of 0.3 µm and a maximum gap of one frame. The minimum duration of tracks was set to 3 frames and only tracks starting and ending during the imaging period were considered. Then, the co-localisation between endoA3 and PSTPIP1 tracks was determined using a custom script written in JMP. To co-localise, tracks had to be within a maximum distance of 0.3 µm. Finally, the mean time of appearance/disappearance was calculated for the co-localising tracks, and the time 0 was arbitrarily defined by the initiation of PSTPIP1 tracks.

4.26 | Statistical analyses

All statistical analyses were performed using GraphPad Prism 7.04 software. D'Agostino–Pearson omnibus normality test was used to check the normality of datasets. If data passed the normality test, parametric tests were used, and data were plotted on graphs as mean ± SEM as error bars. If data did not pass the normality test, nonparametric tests were used, and data were plotted on graphs as median ± 95% CI as error bars. Details on the parametric and nonparametric tests used for each analysis are indicated in figure legends. Significance of comparisons is represented on the graphs by asterisks.

AUTHOR CONTRIBUTIONS

Conceptualisation: Camille Lemaigre, Ulf J. Nilsson, Ludger Johannes, Christian Wunder and Henri-François Renard; Methodology: Camille Lemaigre, Cesar Augusto Valades-Cruz, Ludger Johannes, Christian Wunder and Henri-François Renard; Formal analysis: Camille Lemaigre and Benjamin Ledoux; Investigation: Camille Lemaigre, Apolline Ceuppens and Bastien Vanbeneden; Resources: Mujtaba Hassan, Fredrik R. Zetterberg, Ulf J. Nilsson and Christian Wunder; Writing—original draft preparation: Camille Lemaigre; Writing—review and editing: Ludger Johannes and Henri-François Renard; Visualisation: Camille Lemaigre, Supervision: Henri-François Renard and Pierre Morsomme; Funding acquisition: Ludger Johannes, Henri-François Renard and Pierre Morsomme.

ACKNOWLEDGMENTS

We would like to acknowledge the following people for help in experiments and expertise or providing materials: F. Tyckaert, H. Leffler, D. Durbin and E. Smythe. We thank B. Knoops, P. Dumont and F. Gofflot from LIBST (UCLouvain) for sharing cell culture and flow cytometry facilities and materials. We thank C. Bugli for help concerning statistical analysis. We acknowledge the following imaging core facilities: IMABIOL (LIBST, UCLouvain) and Morph-Im (UNamur). We thank D. Brusa and the Flow Cytometry platform of IREC (UCLouvain). We also would like to acknowledge the Cell and Tissue Imaging Platform (PICT-IBiSA) of the Curie Institute, member of the national infrastructure France-BioImaging and L. Leconte for technical assistance during LLSM acquisitions. Pierre Morsomme is supported by grants from the "Fonds National de la Recherche Scientifique" (FNRS, CDR-J.0119.19) and the "Communauté française de Belgique–Actions de Recherches Concertées" (17/22-085). Henri-François Renard is supported by a Start-Up Grant Collen-Francqui from Francqui Foundation and an Incentive Grant for Scientific Research from the "Fonds de la Recherche Scientifique" (FNRS, MIS-F.4540.21). Camille Lemaigre and Benjamin Ledoux are supported by PhD fellowships from FRIA/FNRS (Belgium). This work was also supported by the France BioImaging Infrastructure (French National Research Agency, ANR-10 INBS-04-07, "Investments for the future"), the Labex DCBiol (ANR-11-LABX-0043) and the Labex Cell(n)Scale (ANR-11-LABX-0038) as part of the Idex PSL (ANR-10-IDEX-0001-02).

CONFLICT OF INTEREST

Ulf J. Nilsson is a shareholder in Galecto Biotech Inc., a company with galectin inhibitors in clinical development.

PEER REVIEW

The peer review history for this article is available at https://publons.com/publon/10.1111/tra.12883.

ORCID

Camille Lemaigre https://orcid.org/0000-0002-9482-9711
Henri-François Renard https://orcid.org/0000-0002-2406-2519
Pierre Morsomme https://orcid.org/0000-0001-7780-7230

REFERENCES

1. Thottacherry JJ, Sathe M, Prabhakara C, Mayor S. Spoiled for choice: diverse endocytic pathways function at the cell surface. *Annu Rev Cell Dev Biol*. 2019;35:55-84.
2. Kaksonen M, Roux A. Mechanisms of clathrin-mediated endocytosis. *Nat Rev Mol Cell Biol*. 2018;19(5):313-326.
3. Chen Y, Aardema J, Misra A, Corey SJ. BAR proteins in cancer and blood disorders. *Int J Biochem Mol Biol*. 2012;3(2):198-208.
4. Frost A, Unger VM, De Camilli P. The BAR domain superfamily: membrane-molding macromolecules. *Cell*. 2009;137(2):191-196.
5. Mim C, Unger VM. Membrane curvature and its generation by BAR proteins. *Trends Biochem Sci*. 2012;37(12):526-533.
6. Safari F, Suetsugu S. The BAR domain superfamily proteins from subcellular structures to human diseases. *Membranes (Basel)*. 2012;2(1):91-117.
7. Doherty GJ, Lundmark R. GRAF1-dependent endocytosis. *Biochem Soc Trans*. 2009;37:1061-1065.
8. Kirchhausen T, Owen D, Harrison SC. Molecular structure, function, and dynamics of clathrin-mediated membrane traffic. *Cold Spring Harb Perspect Biol*. 2014;6(5):a016725.
9. McMahon HT, Boucrot E. Molecular mechanism and physiological functions of clathrin-mediated endocytosis. *Nat Rev Mol Cell Biol*. 2011;12(8):517-533.
10. Boucrot E, Ferreira AP, Almeida-Souza L, et al. Endophilin marks and controls a clathrin-independent endocytic pathway. *Nature*. 2015;517(7535):460-465.
11. Renard HF, Simunovic M, Lemiere J, et al. Endophilin-A2 functions in membrane scission in clathrin-independent endocytosis. *Nature*. 2015;517(7535):493-496.
12. Francis MK, Holst MR, Vidal-Quadras M, et al. Endocytic membrane turnover at the leading edge is driven by a transient interaction between Cdc42 and GRAF1. *J Cell Sci*. 2015;128(22):4183-4195.
13. Lundmark R, Doherty GJ, Howes MT, et al. The GTPase-activating protein GRAF1 regulates the CLIC/GEEC endocytic pathway. *Curr Biol*. 2008;18(22):1802-1808.
14. Sathe M, Muthukrishnan G, Rae J, et al. Small GTPases and BAR domain proteins regulate branched Actin polymerisation for clathrin and dynamin-independent endocytosis. *Nat Commun*. 2018;9(1):1835.
15. Tyckaert F, Zanin N, Morsomme P, Renard HF. Rac1, the actin cytoskeleton and microtubules are key players in clathrin-independent endophilin-A3-mediated endocytosis. *J Cell Sci*. 2022;135(14).
16. Renard HF, Tyckaert F, Lo Giudice C, et al. Endophilin-A3 and Galectin-8 control the clathrin-independent endocytosis of CD166. *Nat Commun*. 2020;11(1):1457.
17. Gallop JL, Jao CC, Kent HM, et al. Mechanism of endophilin N-BAR domain-mediated membrane curvature. *EMBO J*. 2006;25(12):2898-2910.
18. Kjaerulff O, Brodin L, Jung A. The structure and function of endophilin proteins. *Cell Biochem Biophys*. 2011;60(3):137-154.
19. Rao Y, Haucke V. Membrane shaping by the Bin/amphiphysin/Rvs (BAR) domain protein superfamily. *Cell Mol Life Sci*. 2011;68(24):3983-3993.

20. Salzer U, Kostan J, Djinovic-Carugo K. Deciphering the BAR code of membrane modulators. *Cell Mol Life Sci*. 2017;74(13):2413-2438.
21. Gad H, Ringstad N, Low P, et al. Fission and uncoating of synaptic clathrin-coated vesicles are perturbed by disruption of interactions with the SH3 domain of endophilin. *Neuron*. 2000;27(2):301-312.
22. Milosevic I, Giovedi S, Lou X, et al. Recruitment of endophilin to clathrin-coated pit necks is required for efficient vesicle uncoating after fission. *Neuron*. 2011;72(4):587-601.
23. Casamento A, Boucrot E. Molecular mechanism of fast endophilin-mediated endocytosis. *Biochem J*. 2020;477(12):2327-2345.
24. Chan Wah Hak L, Khan S, di Meglio I, et al. FBP17 and CIP4 recruit SHIP2 and lamellipodin to prime the plasma membrane for fast endophilin-mediated endocytosis. *Nat Cell Biol*. 2018;20(9):1023-1031.
25. Tsujita K, Suetsugu S, Sasaki N, Furutani M, Oikawa T, Takenawa T. Coordination between the actin cytoskeleton and membrane deformation by a novel membrane tubulation domain of PCH proteins is involved in endocytosis. *J Cell Biol*. 2006;172(2):269-279.
26. Aspenstrom P. Roles of F-BAR/PCH proteins in the regulation of membrane dynamics and actin reorganization. *Int Rev Cell Mol Biol*. 2009;272:1-31.
27. Akram Z, Ahmed I, Mack H, et al. Yeast as a model to understand Actin-mediated cellular functions in mammals-illustrated with four Actin cytoskeleton proteins. *Cell*. 2020;9(3):672.
28. Shoham NG, Centola M, Mansfield E, et al. Pyrin binds the PSTPIP1/CD2BP1 protein, defining familial mediterranean fever and PAPA syndrome as disorders in the same pathway. *Proc Natl Acad Sci U S A*. 2003;100(23):13501-13506.
29. Yeung YG, Soldera S, Stanley ER. A novel macrophage actin-associated protein (MAYP) is tyrosine-phosphorylated following colony stimulating factor-1 stimulation. *J Biol Chem*. 1998;273(46):30638-30642.
30. Wu Y, Dowbenko D, Lasky LA. PSTPIP 2, a second tyrosine phosphorylated, cytoskeletal-associated protein that binds a PEST-type protein-tyrosine phosphatase. *J Biol Chem*. 1998;273(46):30487-30496.
31. Xu JJ, Li HD, Du XS, et al. Role of the F-BAR family member PSTPIP2 in autoinflammatory diseases. *Front Immunol*. 2021;12:585412.
32. Roberts-Galbraith RH, Gould KL. Setting the F-BAR: functions and regulation of the F-BAR protein family. *Cell Cycle*. 2010;9(20):4091-4097.
33. Chitu V, Pixley FJ, Macaluso F, et al. The PCH family member MAYP/PSTPIP2 directly regulates F-Actin bundling and enhances filopodia formation and motility in macrophages. *Mol Biol Cell*. 2005;16(6):2947-2959.
34. Starnes TW, Bennin DA, Bing X, et al. The F-BAR protein PSTPIP1 controls extracellular matrix degradation and filopodia formation in macrophages. *Blood*. 2014;123(17):2703-2714.
35. Waite AL, Schaner P, Richards N, et al. Pyrin modulates the intracellular distribution of PSTPIP1. *PLoS One*. 2009;4(7):e6147.
36. Homrich M, Gotthard I, Wobst H, Diestel S. Cell adhesion molecules and ubiquitination-functions and significance. *Biology (Basel)*. 2015;5(1):1.
37. Maten MV, Reijnen C, Pijnenborg JMA, Zegers MM. L1 cell adhesion molecule in cancer, a systematic review on domain-specific functions. *Int J Mol Sci*. 2019;20(17):4180.
38. Moos M, Tacke R, Scherer H, Teplow D, Fruh K, Schachner M. Neural adhesion molecule L1 as a member of the immunoglobulin superfamily with binding domains similar to fibronectin. *Nature*. 1988;334(6184):701-703.
39. Maness PF, Schachner M. Neural recognition molecules of the immunoglobulin superfamily: signaling transducers of axon guidance and neuronal migration. *Nat Neurosci*. 2007;10(1):19-26.
40. Faissner A, Kruse J, Nieke J, Schachner M. Expression of neural cell adhesion molecule L1 during development, in neurological mutants and in the peripheral nervous system. *Brain Res*. 1984;317(1):69-82.
41. Nolte C, Moos M, Schachner M. Immunolocalization of the neural cell adhesion molecule L1 in epithelia of rodents. *Cell Tissue Res*. 1999;298(2):261-273.
42. Balaian LB, Moehler T, Montgomery AM. The human neural cell adhesion molecule L1 functions as a costimulatory molecule in T cell activation. *Eur J Immunol*. 2000;30(3):938-943.
43. Angiolini F, Belloni E, Giordano M, et al. A novel L1CAM isoform with angiogenic activity generated by NOVA2-mediated alternative splicing. *Elife*. 2019;8:e44305.
44. Altevogt P, Doberstein K, Fogel M. L1CAM in human cancer. *Int J Cancer*. 2016;138(7):1565-1576.
45. Kiefel H, Bondong S, Hazin J, et al. L1CAM: a major driver for tumor cell invasion and motility. *Cell Adh Migr*. 2012;6(4):374-384.
46. Long KE, Asou H, Snider MD, Lemmon V. The role of endocytosis in regulating L1-mediated adhesion. *J Biol Chem*. 2001;276(2):1285-1290.
47. Kamiguchi H, Long KE, Pendergast M, et al. The neural cell adhesion molecule L1 interacts with the AP-2 adaptor and is endocytosed via the clathrin-mediated pathway. *J Neurosci*. 1998;18(14):5311-5321.
48. Pearse BM, Bretscher MS. Membrane recycling by coated vesicles. *Annu Rev Biochem*. 1981;50:85-101.
49. Hopkins CR, Trowbridge IS. Internalization and processing of transferrin and the transferrin receptor in human carcinoma A431 cells. *J Cell Biol*. 1983;97(2):508-521.
50. Collawn JF, Stangel M, Kuhn LA, et al. Transferrin receptor internalization sequence YXRF implicates a tight turn as the structural recognition motif for endocytosis. *Cell*. 1990;63(5):1061-1072.
51. Pearse BM. Clathrin: a unique protein associated with intracellular transfer of membrane by coated vesicles. *Proc Natl Acad Sci U S A*. 1976;73(4):1255-1259.
52. Motley A, Bright NA, Seaman MN, Robinson MS. Clathrin-mediated endocytosis in AP-2-depleted cells. *J Cell Biol*. 2003;162(5):909-918.
53. Robinson MS. The role of clathrin, adaptors and dynamin in endocytosis. *Curr Opin Cell Biol*. 1994;6(4):538-544.
54. Sweitzer SM, Hinshaw JE. Dynamin undergoes a GTP-dependent conformational change causing vesiculation. *Cell*. 1998;93(6):1021-1029.
55. Dickson TC, Mintz CD, Benson DL, Salton SR. Functional binding interaction identified between the axonal CAM L1 and members of the ERM family. *J Cell Biol*. 2002;157(7):1105-1112.
56. Johannes L, Wunder C, Shafaq-Zadah M. Glycolipids and lectins in endocytic uptake processes. *J Mol Biol*. 2016;24(24):4792-4818.
57. Zetterberg FR, Peterson K, Johnsson RE, et al. Monosaccharide derivatives with low-nanomolar lectin affinity and high selectivity based on combined fluorine-amide, phenyl-arginine, sulfur-pi, and halogen bond interactions. *ChemMedChem*. 2018;13(2):133-137.
58. Stegmayr J, Zetterberg F, Carlsson MC, et al. Extracellular and intracellular small-molecule galectin-3 inhibitors. *Sci Rep*. 2019;9(1):2186.
59. Zetterberg FR, MacKinnon A, Brimert T, et al. Discovery and optimization of the first highly effective and orally available galectin-3 inhibitors for treatment of fibrotic disease. *J Med Chem*. 2022;65(19):12626-12638.
60. Hassan M, van Klaveren S, Hakansson M, et al. Benzimidazole-galactosides bind selectively to the Galectin-8 N-terminal domain: structure-based design and optimisation. *Eur J Med Chem*. 2021;223:113664.
61. Hassan M, Juskaite R, Ströhagen N, et al. Targeting an unexploited binding pocket in Galectin-8 N-terminal domain to discover selective high-affinity LigandsIn preparation 2023.
62. Silberstein C, Lucero MS, Zotta E, et al. A glucosylceramide synthase inhibitor protects rats against the cytotoxic effects of Shiga toxin 2. *Pediatr Res*. 2011;69(5 Pt 1):390-394.

63. Zhao H, Przybylska M, Wu IH, et al. Inhibiting glycosphingolipid synthesis improves glycemic control and insulin sensitivity in animal models of type 2 diabetes. *Diabetes*. 2007;56(5):1210-1218.
64. Jacewicz M, Clausen H, Nudelman E, Donohue-Rolfe A, Keusch GT. Pathogenesis of shigella diarrhea. XI. Isolation of a shigella toxin-binding glycolipid from rabbit jejunum and HeLa cells and its identification as globotriaosylceramide. *J Exp Med*. 1986;163(6):1391-1404.
65. Lingwood C. Verotoxin receptor-based pathology and therapies. *Front Cell Infect Microbiol*. 2020;10:123.
66. Ideo H, Matsuzaka T, Nonaka T, Seko A, Yamashita K. Galectin-8-N-domain recognition mechanism for sialylated and sulfated glycans. *J Biol Chem*. 2011;286(13):11346-11355.
67. Nielsen MI, Stegmayr J, Grant OC, et al. Galectin binding to cells and glycoproteins with genetically modified glycosylation reveals galectin-glycan specificities in a natural context. *J Biol Chem*. 2018;293(52):20249-20262.
68. Traub LM. Tickets to ride: selecting cargo for clathrin-regulated internalization. *Nat Rev Mol Cell Biol*. 2009;10(9):583-596.
69. Janvier K, Kato Y, Boehm M, et al. Recognition of dileucine-based sorting signals from HIV-1 Nef and LIMP-II by the AP-1 gamma-sigma1 and AP-3 delta-sigma3 hemicomplexes. *J Cell Biol*. 2003;163(6):1281-1290.
70. Bonifacino JS, Traub LM. Signals for sorting of transmembrane proteins to endosomes and lysosomes. *Annu Rev Biochem*. 2003;72:395-447.
71. Mason AK, Jacobs BE, Welling PA. AP-2-dependent internalization of potassium channel Kir2.3 is driven by a novel di-hydrophobic signal. *J Biol Chem*. 2008;283(10):5973-5984.
72. Owen DJ, Collins BM, Evans PR. Adaptors for clathrin coats: structure and function. *Annu Rev Cell Dev Biol*. 2004;20:153-191.
73. Kamioka Y, Fukuhara S, Sawa H, et al. A novel dynamin-associating molecule, formin-binding protein 17, induces tubular membrane invaginations and participates in endocytosis. *J Biol Chem*. 2004;279(38):40091-40099.
74. Otsuki M, Itoh T, Takenawa T. Neural Wiskott-Aldrich syndrome protein is recruited to rafts and associates with endophilin A in response to epidermal growth factor. *J Biol Chem*. 2003;278(8):6461-6469.
75. Doherty GJ, McMahon HT. Mechanisms of endocytosis. *Annu Rev Biochem*. 2009;78:857-902.
76. Burns FR, von Kannen S, Guy L, Raper JA, Kamholz J, Chang S. DM-GRASP, a novel immunoglobulin superfamily axonal surface protein that supports neurite extension. *Neuron*. 1991;7(2):209-220.
77. DeBernardo AP, Chang S. Heterophilic interactions of DM-GRASP: GRASP-NgCAM interactions involved in neurite extension. *J Cell Biol*. 1996;133(3):657-666.
78. Bech-Serra JJ, Santiago-Josefat B, Esselens C, et al. Proteomic identification of desmoglein 2 and activated leukocyte cell adhesion molecule as substrates of ADAM17 and ADAM10 by difference gel electrophoresis. *Mol Cell Biol*. 2006;26(13):5086-5095.
79. Gutwein P, Mechtersheimer S, Riedle S, et al. ADAM10-mediated cleavage of L1 adhesion molecule at the cell surface and in released membrane vesicles. *FASEB J*. 2003;17(2):292-294.
80. Weichert W, Knosel T, Bellach J, Dietel M, Kristiansen G. ALCAM/CD166 is overexpressed in colorectal carcinoma and correlates with shortened patient survival. *J Clin Pathol*. 2004;57(11):1160-1164.
81. Sawhney M, Matta A, Macha MA, et al. Cytoplasmic accumulation of activated leukocyte cell adhesion molecule is a predictor of disease progression and reduced survival in oral cancer patients. *Int J Cancer*. 2009;124(9):2098-2105.
82. Kahlert C, Weber H, Mogler C, et al. Increased expression of ALCAM/CD166 in pancreatic cancer is an independent prognostic marker for poor survival and early tumour relapse. *Br J Cancer*. 2009;101(3):457-464.
83. Nabi IR, Shankar J, Dennis JW. The galectin lattice at a glance. *J Cell Sci*. 2015;128(13):2213-2219.
84. Lakshminarayan R, Wunder C, Becken U, et al. Galectin-3 drives glycosphingolipid-dependent biogenesis of clathrin-independent carriers. *Nat Cell Biol*. 2014;16(6):595-606.
85. Lajoie P, Partridge EA, Guay G, et al. Plasma membrane domain organization regulates EGFR signaling in tumor cells. *J Cell Biol*. 2007;179(2):341-356.
86. Partridge EA, Le Roy C, Di Guglielmo GM, et al. Regulation of cytokine receptors by Golgi N-glycan processing and endocytosis. *Science*. 2004;306(5693):120-124.
87. Mathew MP, Donaldson JG. Glycosylation and glycan interactions can serve as extracellular machinery facilitating clathrin-independent endocytosis. *Traffic*. 2019;20(4):295-300.
88. Mathew MP, Donaldson JG. Distinct cargo-specific response landscapes underpin the complex and nuanced role of galectin-glycan interactions in clathrin-independent endocytosis. *J Biol Chem*. 2018;293(19):7222-7237.
89. Johannes L, Jacob R, Leffler H. Galectins at a glance. *J Cell Sci*. 2018;131(9).
90. Sharma DK, Brown JC, Cheng Z, Holicky EL, Marks DL, Pagano RE. The glycosphingolipid, lactosylceramide, regulates beta1-integrin clustering and endocytosis. *Cancer Res*. 2005;65(18):8233-8241.
91. Ferragut F, Vachetta VS, Troncoso MF, Rabinovich GA, Elola MT. ALCAM/CD166: a pleiotropic mediator of cell adhesion, stemness and cancer progression. *Cytokine Growth Factor Rev*. 2021;61:27-37.
92. Shtutman M, Levina E, Ohouo P, Baig M, Roninson IB. Cell adhesion molecule L1 disrupts E-cadherin-containing adherens junctions and increases scattering and motility of MCF7 breast carcinoma cells. *Cancer Res*. 2006;66(23):11370-11380.
93. Hauser S, Bickel L, Weinspach D, et al. Full-length L1CAM and not its Delta2Delta27 splice variant promotes metastasis through induction of gelatinase expression. *PLoS One*. 2011;6(4):e18989.
94. Chen BC, Legant WR, Wang K, et al. Lattice light-sheet microscopy: imaging molecules to embryos at high spatiotemporal resolution. *Science*. 2014;346(6208):1257998.
95. Aguet F, Upadhyayula S, Gaudin R, et al. Membrane dynamics of dividing cells imaged by lattice light-sheet microscopy. *Mol Biol Cell*. 2016;27(22):3418-3435.
96. Jaqaman K, Loerke D, Mettlen M, et al. Robust single-particle tracking in live-cell time-lapse sequences. *Nat Methods*. 2008;5(8):695-702.
97. Lambert T, Shao L. tlambert03/LLSpy: v0.4.3 (0.4.3). Zenodo. 2019.
98. Sofroniew N, Lambert T, Nunez-Iglesias J, et al. napari/napari: 0.4.15 (v0.4.15). Zenodo. 2022.
99. Bolte S, Cordelieres FP. A guided tour into subcellular colocalization analysis in light microscopy. *J Microsc*. 2006;224(Pt 3):213-232.
100. Tinevez JY, Perry N, Schindelin J, et al. TrackMate: an open and extensible platform for single-particle tracking. *Methods*. 2017;115:80-90.

SUPPORTING INFORMATION

Additional supporting information can be found online in the Supporting Information section at the end of this article.

How to cite this article: Lemaigre C, Ceuppens A, Valades-Cruz CA, et al. N-BAR and F-BAR proteins—endophilin-A3 and PSTPIP1—control clathrin-independent endocytosis of L1CAM. *Traffic*. 2023;24(4):190-212. doi:10.1111/tra.12883